Further experimental analysis of undershot water wheels towards the development of a prototype model

Macara, Guilherme; Capelo, Miguel; Ferreira, João; Covas, Dídia

DOI
10.1080/1573062X.2024.2424396

Publication date
2024

Document Version
Final published version

Published in
Urban Water Journal

Urban Water Journal

ISSN: (Print) (Online) Journal homepage: www.tandfonline.com/journals/nurw20

Further experimental analysis of undershot water wheels towards the development of a prototype model

Guilherme Macara, Miguel Capelo, João Ferreira & Dídia Covas

To cite this article: Guilherme Macara, Miguel Capelo, João Ferreira & Dídia Covas (08 Nov 2024): Further experimental analysis of undershot water wheels towards the development of a prototype model, Urban Water Journal, DOI: 10.1080/1573062X.2024.2424396

To link to this article: https://doi.org/10.1080/1573062X.2024.2424396

Published online: 08 Nov 2024.

URBAN WATER JOURNAL
https://doi.org/10.1080/1573062X.2024.2424396

Taylor & Francis
Taylor & Francis Group

RESEARCH ARTICLE

Further experimental analysis of undershot water wheels towards the development of a prototype model

Guilherme Macara[a], Miguel Capelo[a], João Ferreira[b] and Dídia Covas[a]

[a]CERIS, Instituto Superior Técnico, Universidade de Lisboa, Lisbon, Portugal; [b]Department of Water Management, Faculty of Civil Engineering and Geosciences, Delft University of Technology, Delft, Netherlands

ABSTRACT
The current research aims to analyse the effect of the number and shape of the blades and the curvature of the flume bottom on the performance curves of undershot water wheels, based on experimental tests conducted in a fully instrumented laboratory facility. Six wheels are tested: four wheels with plane blades (16, 24, 36, 48) and two with 24 curved blades for two flume bottom configurations. Torque, mechanical power and mechanical efficiency performance curves are determined for several rotational speed and flow rate values. Results demonstrate that the maximum efficiency is achieved for the 36-plane blade wheel, the curved flume bottom reduces water losses under the wheel and increases efficiency, and the blades' shape strongly influences the wheel efficiency. Non-dimensional performance curves are provided to generalise the results. This research provides relevant contributions towards the development of a low-cost energy recovery solution to be applied in water infrastructures.

ARTICLE HISTORY
Received 23 January 2024
Accepted 21 October 2024

KEYWORDS
Water wheels; hydropower; experimental tests; mechanical power

Introduction

The global primary energy demand is projected to increase by over 25% between 2017 and 2040, according to the International Energy Agency (IEA 2017). However, there is a major world concern to reduce and, if possible, eliminate fossil fuel consumption and the emission of greenhouse gases. Several goals and directives have been set to promote energy efficiency and the transition to the use of renewable energy sources (e.g. wind, solar, hydrogen, geothermic). The European Commission, in 2018, established legislation in this regard and the UN (2015) outlined several sustainable development goals (SDG) in the 2030 Agenda concerning climate issues and renewable energy sources (7th and 13th SDG). The share of cumulative power capacity for hydropower is decreasing (IEA 2022), which is limited due to the saturation of large-scale feasible sites that have already been harnessed (Quaranta 2017). Furthermore, the environmental concerns associated with large hydropower plants have spurred the shift towards small hydropower solutions, driven by lower capital costs and reduced environmental impacts (Elbatran et al. 2015).

Small hydropower (SHP) is especially relevant for providing clean energy to rural and remote areas that lack access to electricity grids, particularly in developing countries (Williams and Simpson 2009). These systems are built using simple technology associated with limited civil works (e.g. Archimedes screws), resulting in sustainable solutions with short payback periods (Laghari et al. 2013). However, existing technologies when applied to smaller scales (less than 100 kW) are not always cost-effective, limiting the use of these systems. The installed capacity of SHP is estimated at 75 GW, with an additional 173 GW of potential remaining to be used (Kelly-Richards et al. 2017). The untapped potential can be harnessed by recovering excessive energy from various water infrastructures, including water supply systems (Delgado, Andolfatto, et al. 2019; Delgado, Ferreira, et al. 2019), wastewater systems (Bekker, Van Dijk, and Niebuhr 2022), urban drainage systems (Jorge et al. 2022; Jorge, Do Céu Almeida, and Covas 2021; Ramos et al. 2013, 2021), water and wastewater treatment works and run-of-river applications (Oliveira et al. 2021; Quaranta, Bergamin, and Schleiss 2023).

While much attention has been given to energy efficiency improvements in equipment and processes, less focus has been on energy recovery from existing water and wastewater infrastructures with high flow rates and low available heads. This energy can be harnessed by small hydropower converters, including water wheels, Archimedes screw turbines, hydrostatic pressure machines, and low-head Francis or Kaplan turbines (Quaranta et al. 2022). Recent advancements in pico-hydropower converters have improved these converters' cost-effectiveness. Water wheels can achieve global efficiencies ranging from 60% to 75% with an average investment cost of 5000 €/kW while having minimal environmental impact (Quaranta and Revelli 2016; Quaranta et al. 2022). However, the design of water wheels still relies on methods developed more than a century ago, and there is a lack of up-to-date design information for hydraulic engineers. The availability of a comprehensive 'design handbook' is essential to assess hydropower sources and design water wheels for a wider range of applications (Müller and Kauppert 2004).

Despite hydropower being one of the most used renewable energy sources worldwide, there are still very few systems installed in very low-head sites, in particular at the inlet or outlet of water and wastewater treatment works (Sinagra et al. 2022). Currently, this hydropower

CONTACT Dídia Covas didia.covas@tecnico.ulisboa.pt

potential remains mostly unused since existing energy converters is too expensive for these small applications (Müller and Wolter 2004). One solution for this hydropower segment could be using simple low-cost energy converters, such as the water wheel. In this context, the Group Águas de Portugal (AdP) has launched a challenge to the research team of Instituto Superior Técnico to develop a low-cost, scalable and simple energy harnessing technology to be installed to the outlet or inlet of existing water and wastewater treatment works, being this the main motivation for the development of this research.

Despite much research having been developed on water wheels, the effect of the number and shape of the blades and the flume bottom has not been sufficiently investigated and there is still a lack of water wheel dimensionless curves to be used for a wide range of applications, being these gaps the key drivers for the development of this research.

The current research aims to contribute to a better understanding and the design of water wheels based on an extensive experimental programme conducted in a small prototype assembled at the Laboratory of Hydraulics, Water Resources and Environment, of the Department of Civil Engineering, Architecture and Environment of Instituto Superior Técnico in Lisbon, Portugal. The primary objective is to explore and analyse the mechanical efficiency of undershot water wheels with plane blades to determine the number of blades that maximises the recovered power as well as to assess the effect of the blade shape and the flume bottom on the mechanical efficiency.

For this purpose, six water wheels are tested, including four wheels with plane blades (16, 24, 36, and 48 blades) and two with 24 curved blades for different configurations on the flume bottom (plain and curved). The performance curves of torque, mechanical power and mechanical efficiency are determined as a function of the rotational speed for a set of flow rates. The effect of different water wheel and bottom configurations is discussed. Non-dimensional performance curves are provided to generalise the results. The research findings are critically examined alongside the results from previous studies, providing valuable insights and contextualising the outcomes.

Water wheel types and recent developments

Water wheels can be categorised as horizontal or vertical, depending on the position of the wheel being horizontally or vertically oriented, respectively, and consequently, the axis direction, perpendicular, being aligned in the vertical direction or with a horizontal plane. Vertical water wheels can be further classified as overshot, breastshot and undershot, depending on the water entry position being below, at the level of or above the wheel axle, respectively (Figure 1). In the undershot wheels, water approaches from underneath the wheel's axle, in the breastshot wheels water approaches from the upstream side and in the overshot wheels, the water enters from the top. Breastshot wheels can be further distinguished in high, middle, or low, depending on the position of the water entry relative to the rotation axle. Low breastshot wheels may simply be referred to as undershot water wheels.

Examples of two emblematic undershot waterwheels are presented in Figure 2: the wheel of Cordoba, the Albolafia waterwheel, built in the XII century to collect water to irrigate the Alcázar gardens; and Mouchão wheel with clay buckets, built in 1906 also for irrigation purposes in Tomar, Portugal.

Water wheel technology has witnessed significant advancements to improve their mechanical performance, particularly in the inflow entry, tailrace configuration, blade design, number of blades, and filling ratio, as summarised in the following paragraphs.

The optimal sluice gate opening, a, at the upstream water entry is approximately $a/D = 1/16$, or even $a/H = 1/3$ for experiments conducted with smaller heads (Quaranta and Revelli 2015b, 2016), being D the wheel diameter and H the upstream water height (above the flume bottom in the wheel location). However, for similar conditions, a vertical weir allows the wheel to operate within larger ranges of normalised tangential speeds and is more efficient for lower flow rates. On the other hand, Quaranta argues that regulating the sluice gate opening based on the active flow rate can provide a constant active torque and wheel rotational speeds. This aspect is important as variable speed operation requires costly rectifier/control/inverter systems and expensive gearboxes (Müller and Kauppert 2004).

According to Müller and Wolter (2004), the inflow should be designed as a weir inflow with an angle of 45–50° with the

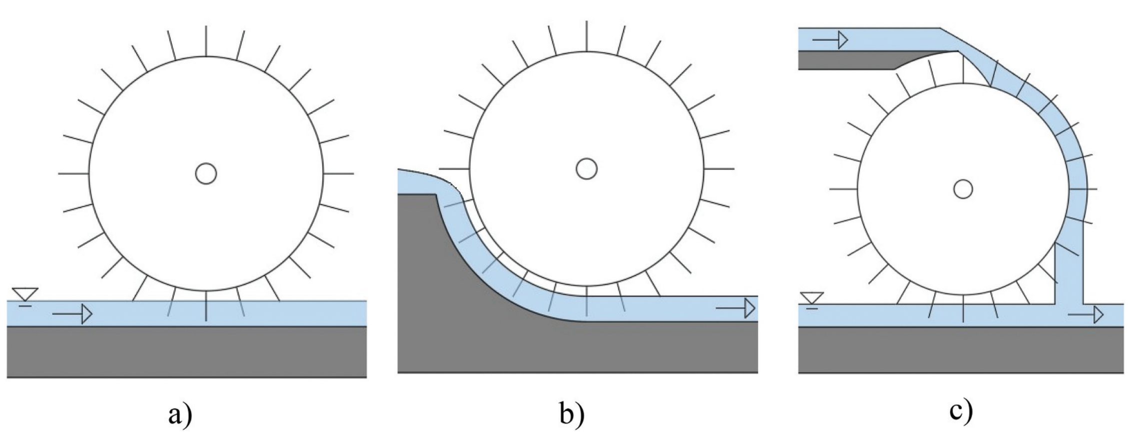

Figure 1. Vertical (or horizontal axle) water wheels: (a) Undershot; (b) Breastshot; (c) Overshot.

(a) (b) (c)

Figure 2. Emblematic undershot waterwheels: (a)-(b) Islamic vertical water wheel in Cordoba, Spain; (c) Mouchão water wheel with clay buckets in Tomar, Portugal.

horizontal, resulting in effective entry angles (striking the blade) of 0–15º (45º inflow) to 7–20º (50º inflow angle). Effective entry angles of 0–20º strike a balance between utilising potential energy and minimising losses at the inflow. This finding is supported by Kodirov and Tursunov (2019), who identified an optimal effective entry angle of 15º. Inflow weirs allow for better management of upstream water depths and enable the exploitation of a wider range of flow rates. This modification can increase efficiency from 78% to 81.5% according to Müller and Kauppert (2004), or even from 42% to 67% according to Helzimar (2016). Weirs also provide higher flow resistance than the assumed in design calculations, leading to higher upstream water depths than those expected, and weir inflows are less prone to blockage and simpler to construct.

The tailrace hinders vertical water wheels when the blades push against the flow. To optimise turbine wheel performance, the downstream water depth should be adjusted to the lowest point of the wheel hub (Helzimar 2016). In addition, Müller and Wolter (2004) suggests that an inclined tailrace, with a length of 1 m and an inclination of 6/1000 (which corresponded to 1.2% of the total head), can increase efficiency from 81.5% to 87.3%. An inclined tailrace, which allows water to be carried away by its weight, is therefore essential for efficient water wheels.

The blade design criteria should consider three principles to minimise energy losses (Quaranta and Revelli 2017a). Firstly, the relative entry stream velocity at the blade's impact point should align with the blade inclination to reduce inflow power losses. Secondly, the uplift of water downstream of the wheel and outflow power losses should be minimised by ensuring the blades exit at a normal angle or with a backward inclination relative to the tailrace's free surface, reducing drag. The ratio of blade depth to wheel diameter (l/D) is widely accepted as equal to 0.2 (a common ratio in literature for undershot and breastshot water wheels) and the effective entry angle of 0–20º generally shows a better performance. CFD simulations have shown that a circular blade profile improves wheel performance by an average of 4% compared to quasi-elliptical profiles (Quaranta and Revelli 2017a).

The optimal number of blades depends on the kinetic and potential energy harvested from the flow, as well as the counterbalanced energy losses from blade-flow and water-blade impacts (Quaranta and Revelli 2015b). CFD simulations for undershot water wheels indicated an optimal number of 16 blades (Sari et al. 2022), while for overshot water wheels, simulations suggested a peak efficiency at 48 blades (Quaranta and Revelli 2017b), with an average error of less than 6% compared to experimental tests. In some experiments, the performance of Zuppinger and Sagebien wheels remained optimal even with a reduced number of blades, specifically 30 instead of the 70–80 recommended in historical literature (Quaranta and Müller 2018; Quaranta and Revelli 2018). However, reducing the number of blades below a certain minimum value resulted in increased volumetric losses and leakage. Thus, a trade-off exists, as at least three blades should be simultaneously in contact with water (Quaranta 2017). The filling ratio refers to the ratio of the water volume between a pair of blades to their maximum volume capacity. The agreed filling ratio for buckets in breastshot and overshot water wheels is generally between 0.3 and 0.5. However, for mid-breastshot wheels, the filling ratio can be extended up to 0.90, as the optimum filling ratio increases with higher flow rates (Quaranta and Müller 2018). The optimal filling ratio depends on all the features of the wheel previously explained as well as on the flow rate, the available hydraulic head and the rotational speed.

Data collection programme

Experimental facility

Experimental tests are carried out in a pipe-rig assembled at the Laboratory of Hydraulics, Water Resources and Environment of Instituto Superior Técnico, Lisbon, Portugal. The system is composed of a 40 cm diameter wheel installed in a horizontal flume, with a water-recirculating pipe circuit. The facility is fully equipped with instrumentation to measure hydraulic and mechanical parameters, including an ultrasonic flow meter, two pressure transducers, one torque sensor and one rotational speed sensor. The data acquisition system is composed of two National Instruments^{TM} acquisition boards (type NI cDAQ9178) used to capture the electrical input signals from the sensors and to transmit them to a laptop computer. Figure 3 highlights several components of the assembled test-rig.

The test rig consists of a small acrylic flume with a rectangular cross-section with 18 cm of width, 25 cm of height and a total length of 1.56 m. In the flume section, where the water wheels are tested, the width and height are reduced to 11.7 cm and 23 cm,

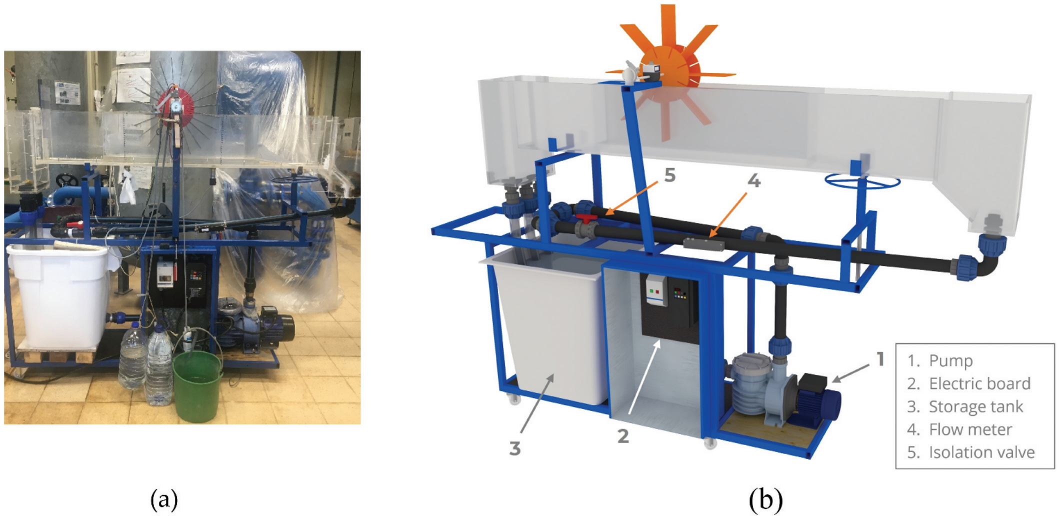

Figure 3. Test-rig for collecting the experimental investigation: (a) photo; and (b) schematic representation.

respectively, by inserting removable 3 cm-thick acrylic plates; this reduction allowed to test smaller size wheels whose shaft, connecting lateral plates and blades could be printed in a small 3D printer. A closed loop raising pipe system made of high-density polyethylene (HDPE), of pressure class PN10, with a total length of 3.60 m and a nominal diameter of 40 mm (inner diameter of 34 mm), is used to recirculate the water. Water is pumped from a 120 L storage tank by a centrifugal pump KSB^{TM} model Filtra N 24D, with a rated power of 1.8 kW, capable of delivering a maximum flow rate of 8 L/s and a maximum pressure head of 19 m. A plastic curled-up net is installed at the inlet section of the flume to stabilise the flow as well as to dissipate the pressure in excess. This net also helps to create favourable conditions for the experimental setup, namely, a steady water surface and less turbulence. The maximum flow rate of the pipe system is 3.9 L/s, limited both by the pump characteristics and by the local head losses caused by the four 90º curves existing in the raising pipe. A variable speed drive (Omron Hitachi^{TM} Jx Inverter) is installed on the pump to control the flow rate.

Several water wheels are tested with different number (16, 24, 36, 48) and curvature (plain and curved) of blades and configuration of the flume bottom. The main dimensions of the wheel and of the flume cross-section are presented in Table 1 and Figure 4.

Table 1. Flume and wheel dimensions.

Component	Dimensions	Units	Values
Flume (cross-section)	Flume width, B	m	0.117
	Flume height, h	m	0.230
Wheel dimensions	Wheel diameter, D	m	0.482
	Shaft diameter, D_s	mm	8
	Hub diameter, D_h	m	0.100
Blade dimensions	Blade width, B_b	m	0.105
	Blade length, l	m	0.160
	Blade thickness, t	mm	3
Gaps between the wheel and the flume walls	Bottom gap, g_b	mm	4
	Lateral gap, g_w	mm	6

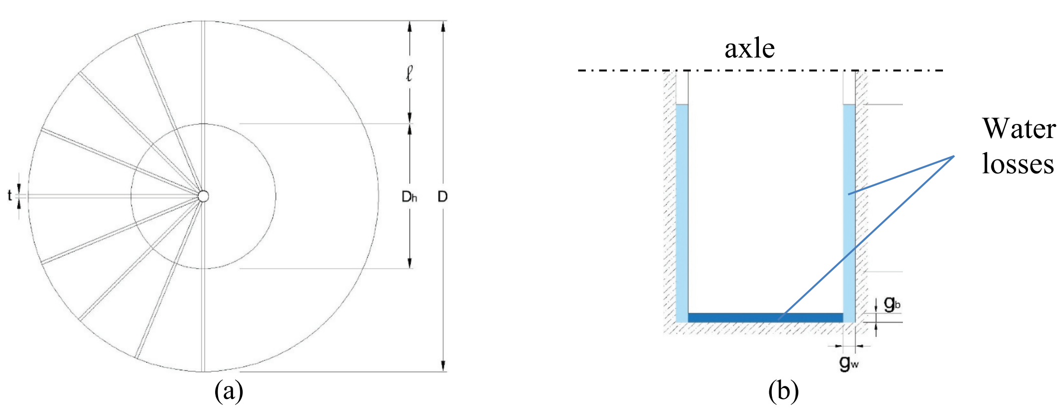

Figure 4. Schematic representation of the tested undershot water wheel: (a) lateral view and (b) cross-section view.

Measurement equipment

The facility is fully equipped with instrumentation for measuring hydraulic and mechanical parameters, namely with two strain-gauge pressure transducers Figure 5(a,b) to measure the upstream and the downstream water depth, one torque transducer Figure 5(c), one tachometer Figure 5(d) and one non-intrusive ultrasonic flow meter Figure 5(e,f). The technical specifications and the uncertainty of each sensor are presented in Table 2.

The sensors are connected to a data acquisition system using two National Instruments™ boards (type NI cDAQ9178) which acquire the electrical input signals and transfer them into a computer that collects and processes data using a Test-Hydro, a platform developed in LabView specifically for turbomachines testing (Figure 6).

All instrumentation has been tested and calibrated before conducting each set of tests, by comparing collected data with that obtained by an independent measurement, except data collected by the torque sensor. This allowed to ensure the minimisation of potential measurement errors.

Experimental tests

Two sets of experimental tests are conducted, testing a total of six different wheels: the first set (Set I) includes four wheels with plane blades (16, 24, 36, and 48 blades, referred as I16, I24, I 36 and I48), while the second includes two wheels with the same number of curved blades (24 blades), but with different flume configuration bottoms: a horizontal bottom (II24) and a curved bottom (III24). The first set of tests aimed to analyse the effect of the number of blades in the harnessed power. The second set of tests aimed to critically analyse the influence of various configurations identified in the literature on the wheel behaviour, namely, by changing the curvature of the blades and the shape of the upstream water entry. The blade curvature is not optimised. Experimental tests are conducted for rotational speeds ranging from 3 to 21 r.p.m.

Figure 7 shows six tested wheels operating for the same rotational speed of 11.5 r.p.m. and flow rate of 2.23 L/s. Different upstream water depths are observed, as the higher number of blades increases the flow resistance, the harnessed power and, consequently, the upstream water depth (compare Figure 7(a-d)). The tested curved blades introduced additional flow turbulence and tended to reduce the harnessed power and the wheel efficiency (compare Figure 7(b) with e-f).

The wheel axle is equipped with a brake system designed to control the rotational speed by creating a resisting torque on the wheel shaft using adjustable weights (Figure 8). This brake system, combined with the variable speed drive that regulates the flow rate in the supply pump, allows establishing the balance of the angular momentum in the wheel and, thus,

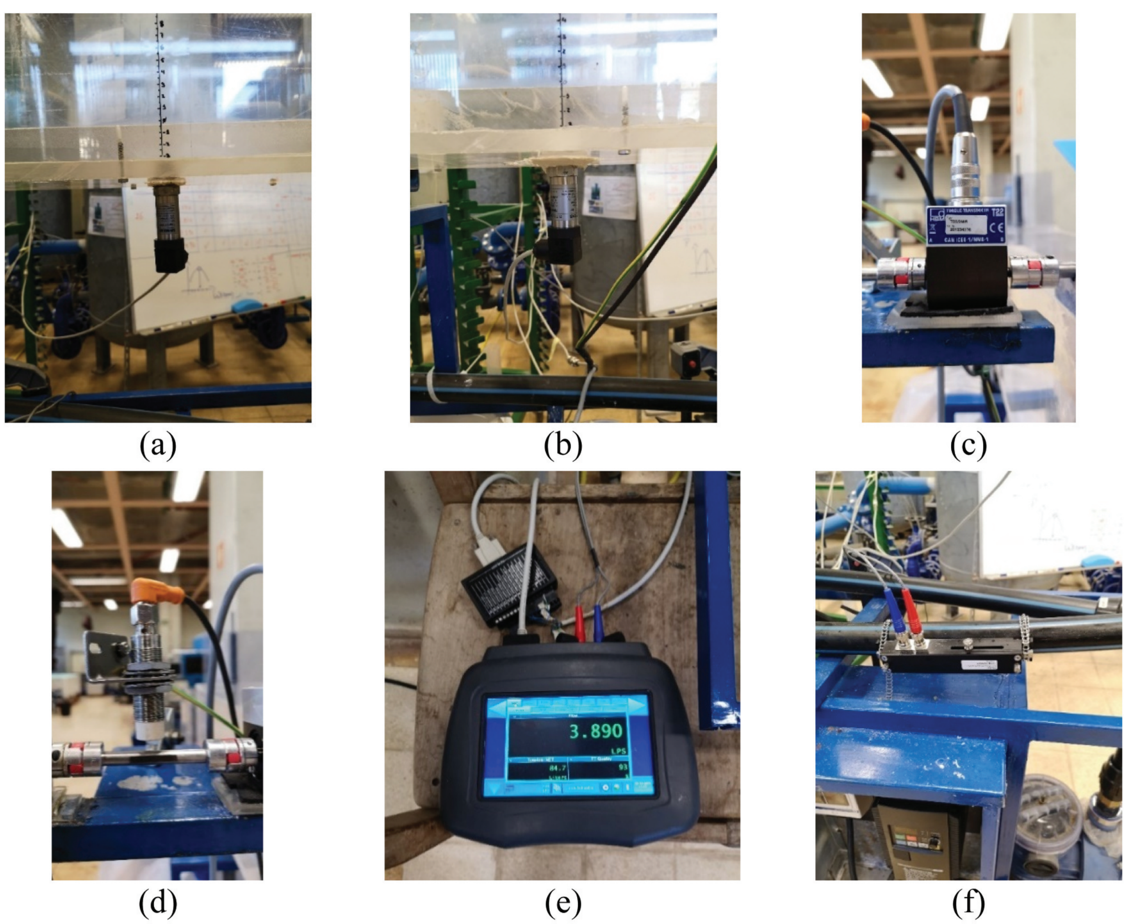

Figure 5. Measurement equipment: (a) upstream pressure transducer; (b) downstream pressure transducer; (c) torque transducer; (d) tachometer; ultrasonic flow meter: (e) display system and (f) transducer.

Table 2. Measurement equipment characteristics.

ID	Measured parameter	Sensor type	Measurement range	Units	Accuracy
Q	Flow rate	DXN Portable Ultrasonic Flowmeter	[0, 12]	m^3/s	±1% of span
p_u	Upstream pressure	Siemens SITRANS P Serie Z	[0, 0.25]	bar	±0.25% of span
p_d	Downstream pressure				
T	Torque	HBM: T22/2Nm	[−2, +2]	Nm	±0.5% of full scale
N	Rotational speed	GM205	0 - 1200	r.p.m.	±0.25% of span

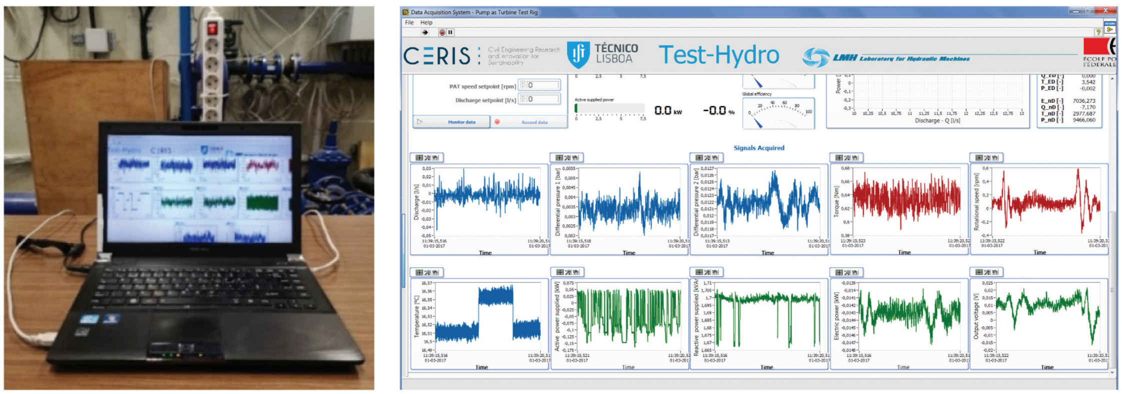

Figure 6. Test-hydro interface: a platform for collecting and visualizing multiple sensor data collection used in this research (Delgado 2018).

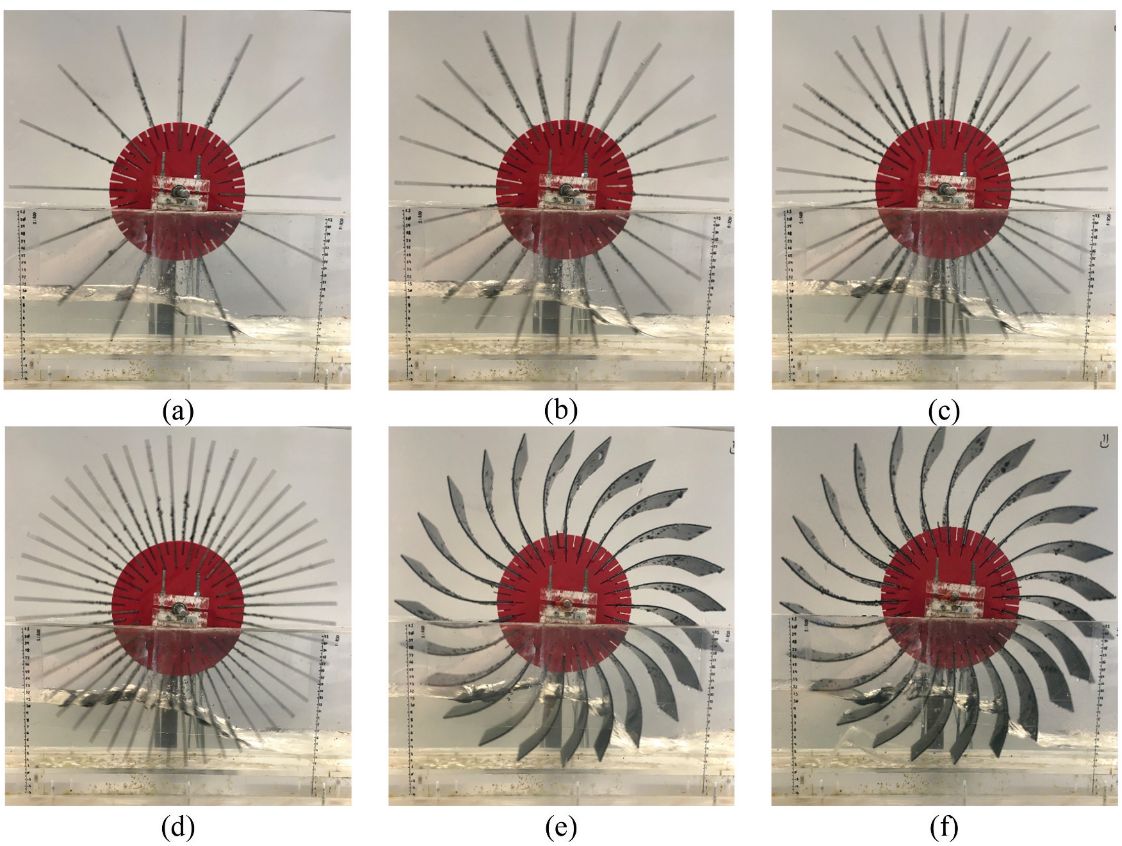

Figure 7. Tested undershot water wheels for $N = 11.5$ r.p.m. and $Q = 2.23$ L/s: (a) 16 plane blades (I16); (b) 24 plane blades (I24); (c) 36 plane blades (I36); (d) 48 plane blades (I48); (e) 24 curved blades with plain bottom (II24) and (f) 24 curved blades with an upstream bottom platform (III24).

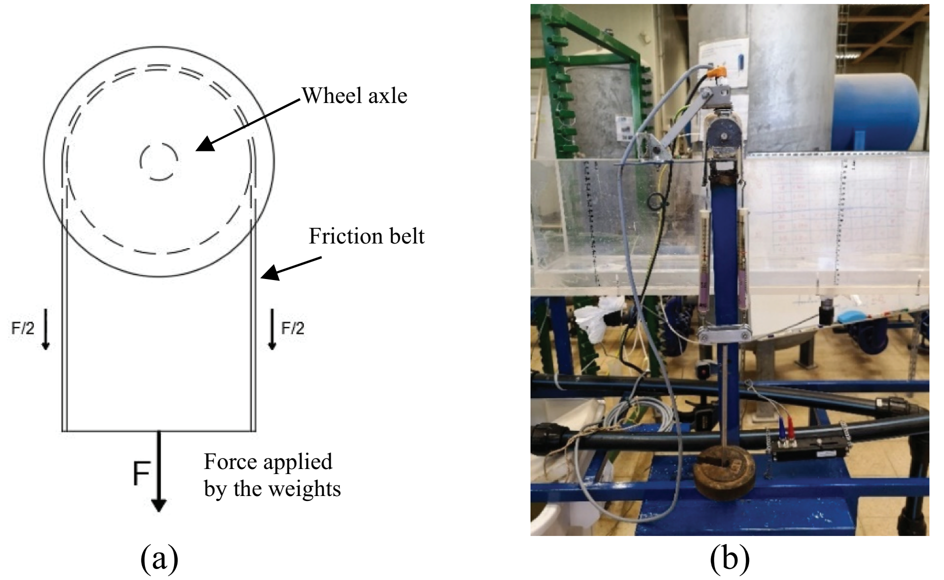

Figure 8. Brake system of the experimental facility: (a) initial sketch; (b) installed system.

adjusting the rotational speed. The rotational speed is set by the brake system by using adjustable weights to apply friction force to the shaft of the wheel. To ensure a comprehensive coverage of operating conditions, tests are conducted for each water wheel and flow rate for a minimum of six rotational speeds (3 to 21 r.p.m.), where higher flow rates are associated with higher rotational speeds.

During each test, data are collected for a time frame of 30 s with a sampling rate of 500 hz. This involved the recording of 15,000 data points of each measured parameter (*i.e.*, flow rate, upstream and downstream pressure-head, torque, and rotational speed). In each test, each of the five parameter values are calculated based on the ensembled average of collected time series to filter the time series oscillations associated with the blades, the rotational speed and flow turbulence.

A set of 243 experimental tests are carried out: *ca*. 48 tests for each wheel with plane blades (I) and 26 tests for each wheel with curved blades (II and III). Two tests are selected to show the recorded signal pulsation (see raw data in Figure 9). The first refers to the wheel with 16 plane blades (I16) for a flow rate of 2.57 L/s and a rotational speed of 9.7 r.p.m. (ca. 10 r.p.m.). The second refers to the wheel with 36 plane blades (I36) for a flow rate of 3.24 L/s and a rotational speed of 13.3 r.p.m. (ca. 13.5 r.p.m.). Treated data for the six tested wheels are presented in Tables A1–A6, in Appendix A.

As illustrated in Figure 9, the upstream and downstream water pressure at the bottom of the flume, p_u and p_d, as well as the torque, T, have a regular oscillating pattern that repeats for each rotation of the water wheel, while the flow rate, Q, does not since this parameter is ensured by the supply pump and, thus, it is hardly influenced by the wheel rotation (though, a minor influence exists due to water level variation that affects pump head). The rotational speed is expected to exhibit the same periodicity, although it is not depicted as the data are recorded only once per revolution and are not affected by the blade rotation frequency. Based on the mean rotational speed presented in Figure 9(e), the expected periodicity of these parameters is *ca*. 6 and 4.5 s, respectively, for I16 and I36. This pattern arises from the resistance created by the water wheel, where certain sections, such as specific blades, experience increased flow blockage. The flow rate experiences a 2 s delay caused by the 3.60 m pipe, leading to a different periodicity. The flowmeter is installed in the middle of the pipe, causing an additional time lag of 1 s.

Analysis of experimental results

Hydraulic parameters

The water depths correspond to the pressure-heads of the fluid at the bottom of the flume, $h = p/\gamma$, being p the pressure and γ the specific weight of water, collected by the transducers installed at the upstream and the downstream ends of the water wheel. None of these water depths exceeds the blade length (16 cm, cf. Table 1).

Figure 10 shows an example of the measurements water depths collected for the 16-plain blade wheel for different flow rates, Q, and rotational speeds, N. The upstream water depth, h_u, decreases from 0.16 to 0.05 m (being 1.5 to 5.5 times the critical water) with the increase of the rotational speed (for constant Q), since less resistance is imposed in the wheel axle and, thus, less head difference between upstream and downstream is created. The upstream water depth also increases with the flow rate increase (for constant N) since more water is flowing and creating a higher head loss in the wheel section. Conversely, the downstream water depth, h_d, increases with the rotational speed increase (for constant Q) and with the flow rate increase (for constant N), varying between 0.02 and 0.045 m, being always below the critical water depth. The highest rotational speeds for each flow rate correspond to the null friction imposed in the wheel axle by the brake system, having only the friction inherent to the axle supports.

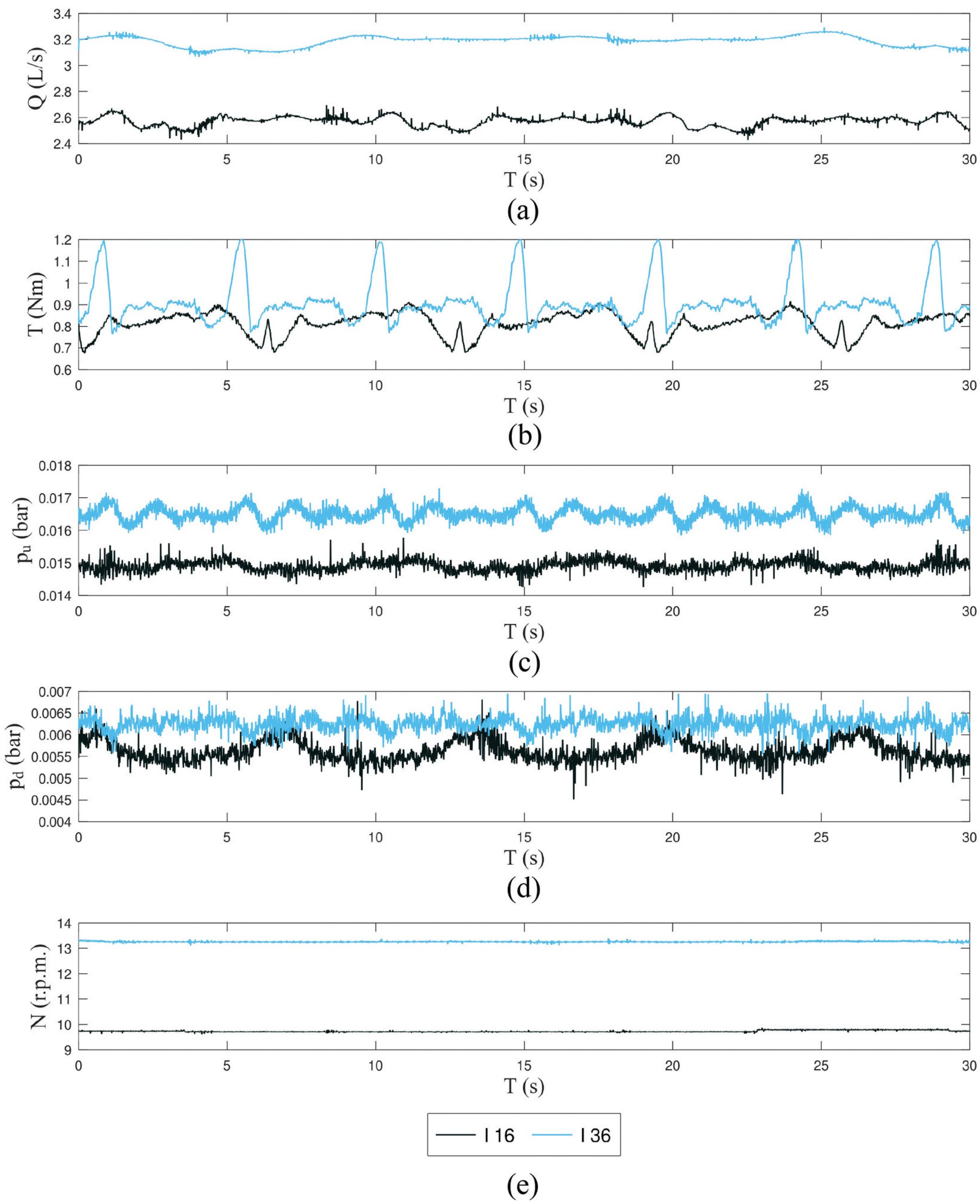

Figure 9. Raw data of experimental tests I16 (Q = 2.57 L/s, N = 10 r.p.m.) and I36 (Q = 3.24 L/s, N = 13.5 r.p.m.): (a) flow rate; (b) torque; (c) upstream water pressure-head; (d) downstream water pressure-head; (e) rotational speed.

The total head, H, is calculated based on the measured pressure and flow rate and the physical characteristics of the flume, as follows:

$$H = z + \frac{p}{\gamma} + \frac{Q^2}{2gS^2} \tag{1}$$

where z is the elevation of the flume bottom at the measurement section, $\frac{p}{\gamma}$ is the pressure-head at the flume bottom, p is the pressure, γ is the specific weight of water, Q is the flow rate S is the water cross-sectional area ($S = Bh$), B is the flume width and h is the water depth. The reference elevation ($z = 0$) corresponds to the bottom of the flume, which was ensured to be horizontal, thus the total head is equivalent to the specific head.

The hydraulic power, P_h, of a water wheel describes the power available in the flow to be harvested by the wheel but does not account for the leakage between the wheel and the flume walls/bottom, nor head losses due to friction and turbulence. The hydraulic power depends on the flow rate, the upstream and downstream water depths, and the physical characteristics of the flume, as follows:

$$P_h = \rho g Q (H_u - H_d) \tag{2}$$

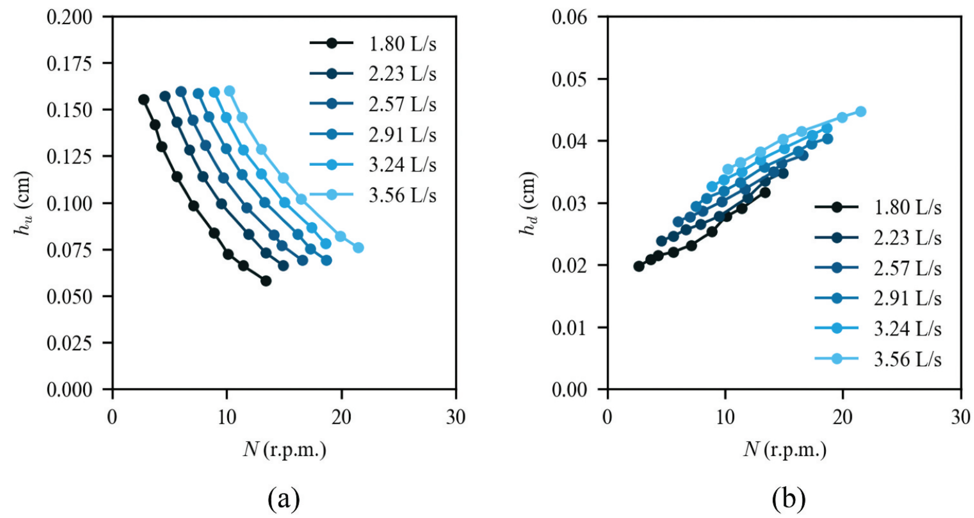

Figure 10. Measured water depths for the 16-blade wheel: (a) upstream water depth; (b) downstream water depth.

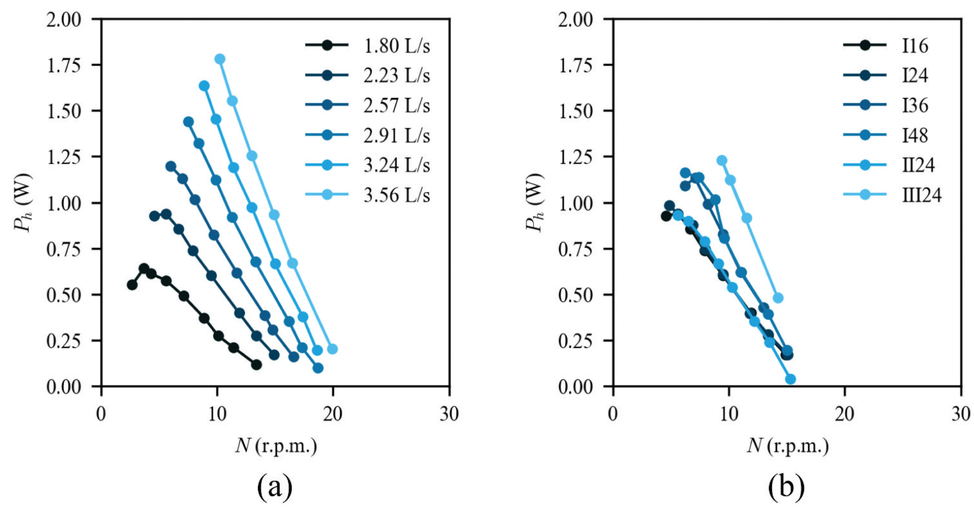

Figure 11. Hydraulic power for (a) the 16-blade wheel; and (b) the six wheels for $Q = 2.23$ L/s.

where $P_h$the hydraulic power, ρ is the water density (1000 kg. m^3), H_u and H_d are the upstream and downstream total head values (equivalent to specific head values since the flume is horizontal) calculated by Equation (1). This parameter corresponds to the maximum available power for a given head and flowrate, if no water and friction losses exist.

Figure 11(a) shows that the hydraulic power decreases with the increase of rotational speed for each flow rate and increases with the increase of flow rate for a fixed rotational speed. Figure 11(b) demonstrates that the hydraulic power also increases with the number of blades for the same rotational speed (compare I16-I48), with the curvature of the blades (compare I24 with II24) and for the curved flume platform (compare II24 with III24). These results demonstrate that the geometry of the wheel (number and curvature of blades) and the flume upstream platform have a major effect on the available hydraulic power.

Mechanical parameters

Mechanical parameters, such as torque, power and efficiency, are analysed herein. The torque, T, a directly measured parameter, represents the rotational force generated by the flow momentum and the hydrostatic force of the fluid on the wheel blades, being balanced by frictional torque created by the brake system applied in the wheel shaft. The mechanical power, P, refers to the actual work (or energy) that is transferred to the wheel axle per unit of time. This parameter is calculated based on measured torque and rotational speed values. It is typically described by:

$$P = T \cdot \omega \qquad (3)$$

where P is mechanical power (W) and ω is the angular speed (rad/s). Considering that $\omega = N \cdot \frac{60}{2\pi}$, being N is the rotational speed (r.p.m.), it can also be calculated as:

$$P = T \cdot N \cdot \frac{60}{2\pi} \tag{4}$$

The angular speed and the rotational speed depend on the flow rate while the upstream and the downstream water depths depend on the physical characteristics of the flume and of the wheel. The increase in the torque is associated to the decrease in the rotational speed. Thus, there is a point at which the increase in the torque is counter-balanced by the decrease in the rotational speed, resulting in the maximum mechanical power. Additionally, the wheel does not generate any power in two conditions: when it is static (*i.e.,* $N = 0$), and when it rotates without friction in the axle, that in a free-wheel state (*i.e.,* $T = 0$).

The mechanical efficiency, η, quantifies how much of the available hydraulic power is effectively converted into mechanical power, being given by $\eta = \frac{P}{P_h}$ where P is the mechanical power (Eq. (4)) and P_h is the hydraulic available power (Equation (2)). The wheel cannot convert all the available hydraulic power into mechanical power due to several losses in the system, such as (i) the flow turbulence losses, which depend on the number and shape of the wheel blades and the curvature of the flume bottom; (ii) the leakage losses, associated with the flow rate that passes between the blades and the flume bottom and walls, decreasing the effective flow rate that generates mechanical power; (iii) the impact losses, created by the impact of the blades with the tailrace and by the impact of the entry water on the blades; and (iv) the inevitable friction losses in the wheel shaft created by the supports and the connections. Therefore, optimising the wheel geometry (number and shape of the blades) and the flume bottom upstream of the wheel can significantly improve the hydraulic efficiency of the water wheel system.

The performance curves of the torque, mechanical power and mechanical efficiency as a function of the rotational speed for each of the four wheels with plane blades are presented in Figure 12. Before pursuing the analysis, it should be noted that the representation of the performance curves as a function of the rotational speed (instead of the flow rate) is not the most common representation, despite being physically equivalent and other authors have also used this representation (Quaranta and Revelli 2015a). However, during the experimental tests, it was easy to control the flow rate and to keep it constant by regulating the variable speed drive of the supply pump, whereas it was difficult to keep the rotational speed constant because it was controlled by the frictional mechanism applied in the wheel axle. Thus, it was not possible to obtain points of 'measured parameter as a function of the flow rate' for constant values of rotational speeds, because the latter was not constant. Representing the performance curves as a function of the flow rate based on collected data would require interpolations and curve fittings to obtain those curves. Also, the measurement points would be lost, and unnecessary uncertainty would be introduced in the analysis.

The torque decreases with the increase of rotational speed, for a constant flow rate, and increases with the increase of flow rate, for a constant rotational speed. The torque is null ($T = 0$) for the freewheel condition (i.e. the wheel with no resistance in the axle), which corresponds to the maximum rotational speed, varying between 15 and 23 r.p.m depending on the number of blades and flow rate. The maximum torque is limited by the maximum range of the torque sensor (*i.e.*, 2 Nm), as wheel as by the upstream water depth, whenever it exceeds the size of the blades (*i.e.*, 0.16 m).

The mechanical power has a similar behaviour to the torque, decreasing with the increase of the rotational speed and increasing with the increase of the flow rate. However, the mechanical power performance curves for the lowest flow rate (1.83 L/s) have a maximum peak value which is associated with the maximum torque (2 Nm). This is not observed for higher flow rates, since the upstream water depth exceeds the blade size (16 cm, see Figure 10(a)) and the water overflows the blade; thus, the maximum measurable torque is not reached and the maximum power is not attained. Indeed, these maximum values are expected to occur in each power curve, as the wheel does not generate any power for the static conditions (*i.e.,* $N = 0$). The mechanical power of the freewheel is almost but not null (as expected); this residual value is due to the frictional forces in the wheel shaft and the surfaces of the blade that cannot be avoided in the tests.

The mechanical efficiency curves have a curved shape with a maximum value for a particular rotational speed that depends on the flow rate and the wheel configuration. The maximum efficiency values (50–60%) as well as the associated rotational speeds (10–15 r.p.m) increase with the increase of the flow rate. These curves tend to zero when the wheel is static (*i.e.,* $N = 0$) or when it is in a free-wheel state (*i.e.,* $T = 0$).

Figure 13 presents the performance curves obtained for the 24-curved blade wheel without and with a curved platform at the flume entry for four flow rates. The performance curves follow the same trend as refered, though with minor differences. Maximum (2 Nm) and minimum (0 Nm) torque values are not observed, as major turbulence is generated by the impact of the blades on the water surface that creates major head losses and dissipates part of the generated energy. Maximum power is lower than for the 24-plane blade wheel for the same reasons and, consequently, maximum mechanical efficiencies are lower, though the curved flume entry allows to partially compensate for the impact losses by reducing leakage losses between the blade and the flume walls/bottom.

Mechanical parameters analyses

A comparison of the performance curves obtained for the six different wheel/flume configurations is presented herein, namely the analysis of the effect of the number of blades, the shape of the blades and the curvature of the flume entry platform.

Effect of the number of blades

The effect of the number of blades in the performance curves is illustrated in Figure 14 for the minimum (*i.e.*, 1.83 L/s) and the maximum (*i.e.*, 3.56 L/s) values of the flow rate and for the wheels with plane blades. In general, increasing the number of blades, for a constant rotational speed, tends to increase the torque and the mechanical power. However, this is not

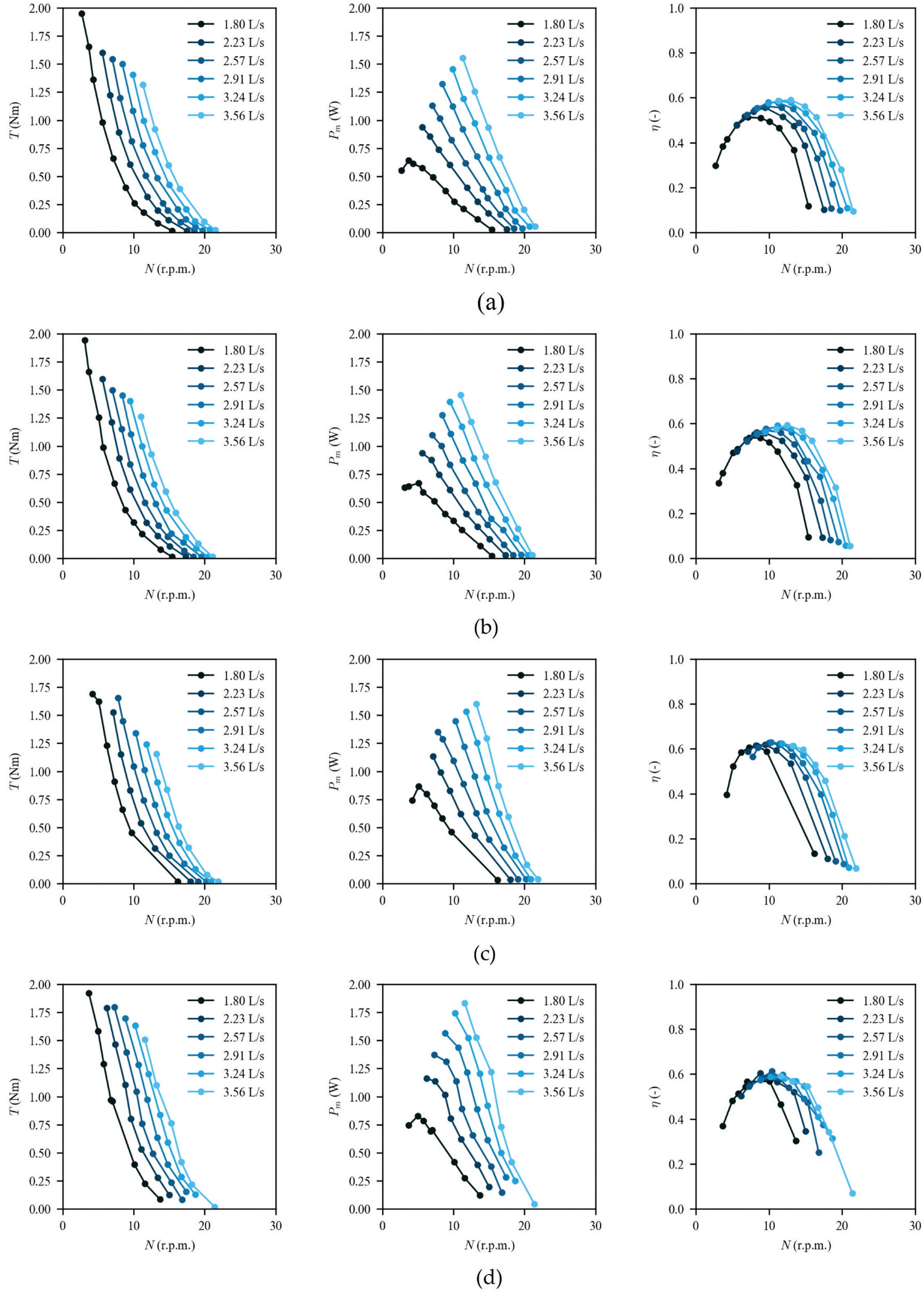

Figure 12. Experimental performance curves of the plane-blade wheels (torque, mechanical power and efficiency): (a) 16-blade wheel (I16); (b) 24-blade wheel (I24); (c) 36-blade wheel (I36); (d) 48-blade wheel (I48).

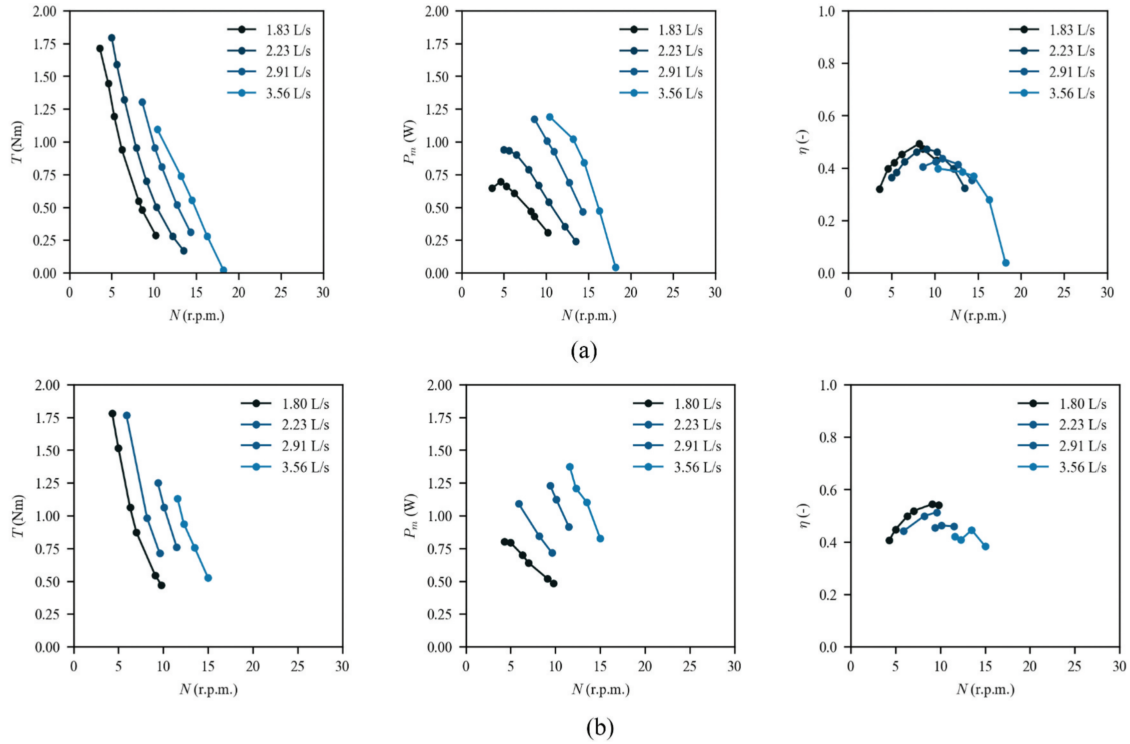

Figure 13. Experimental performance curves of the 24 curved-blade wheels (torque, mechanical power and efficiency): (a) horizontal flume bottom (II24); (b) flume with a curved platform at the wheel entry (III24).

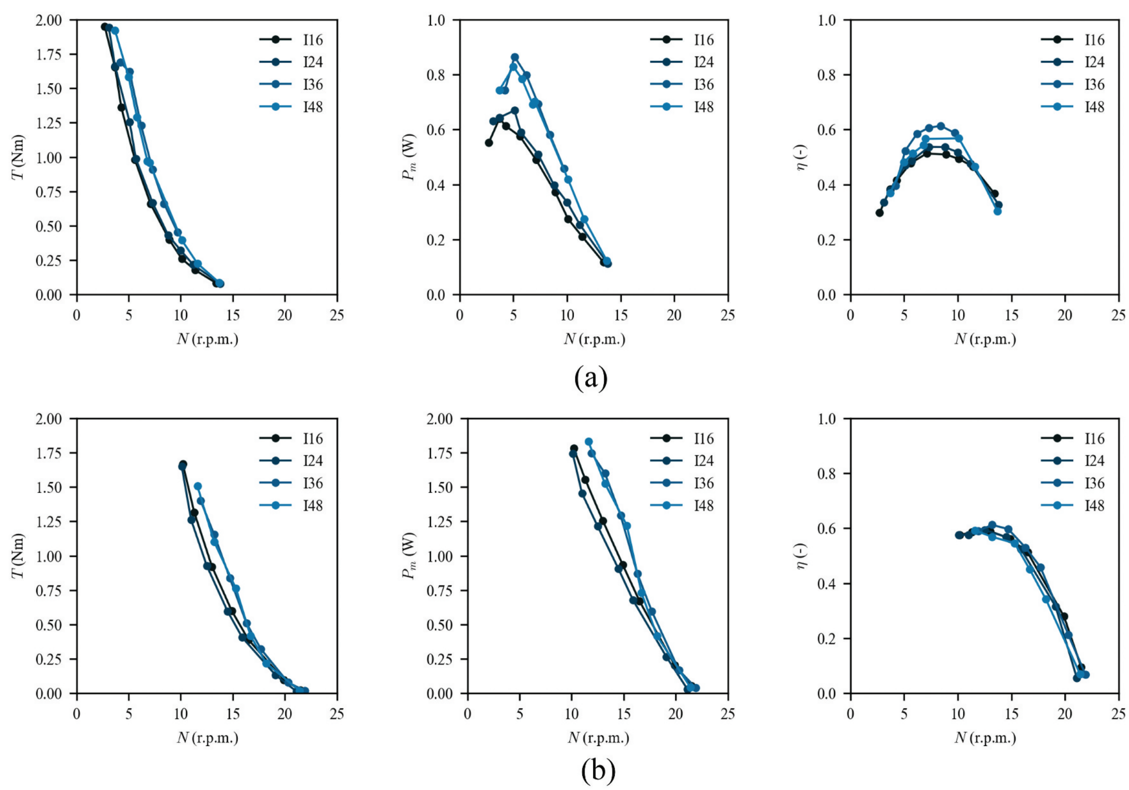

Figure 14. Experimental performance curves for the 16, 24, 36 and 48 plane blade wheels (torque, mechanical power and efficiency): (a) $Q = 1.83$ L/s and (b) $Q = 3.56$ L/s.

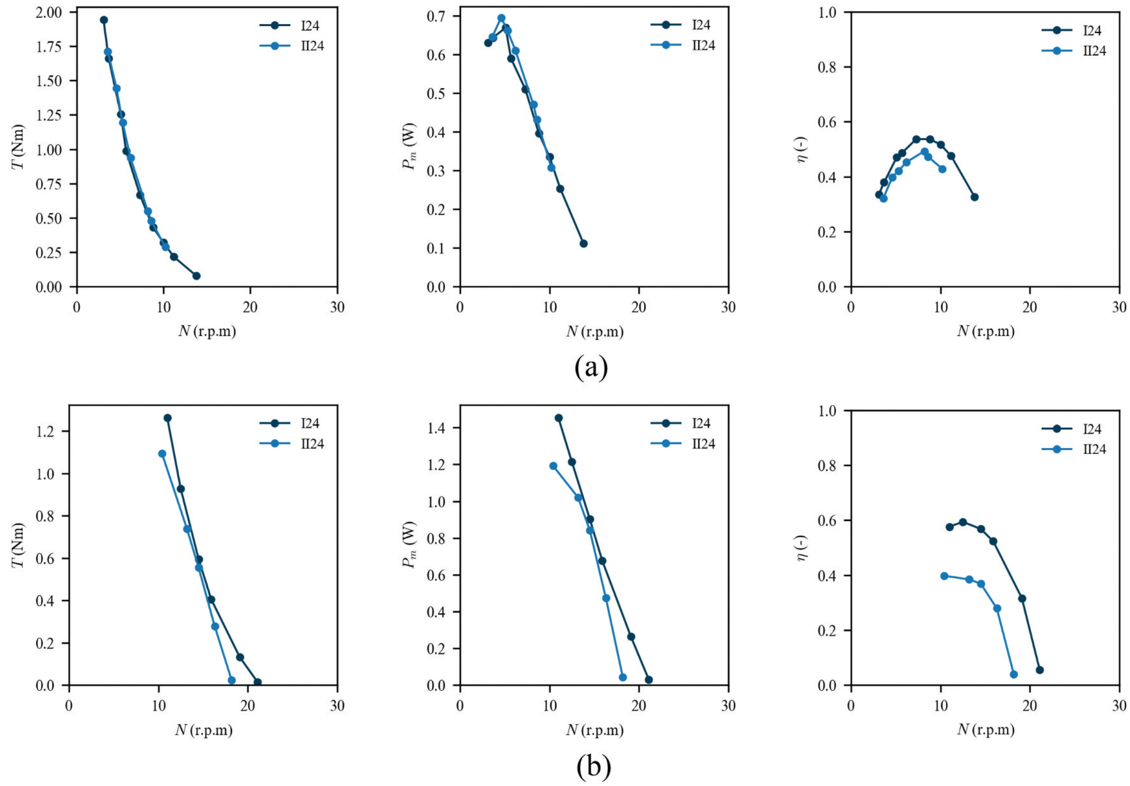

Figure 15. Experimental performance curves 24 plane and 24 curved blade wheel (I24 and II24) (torque, mechanical power and efficiency): (a) Q = 1.83 L/s and (b) Q = 3.56 L/s.

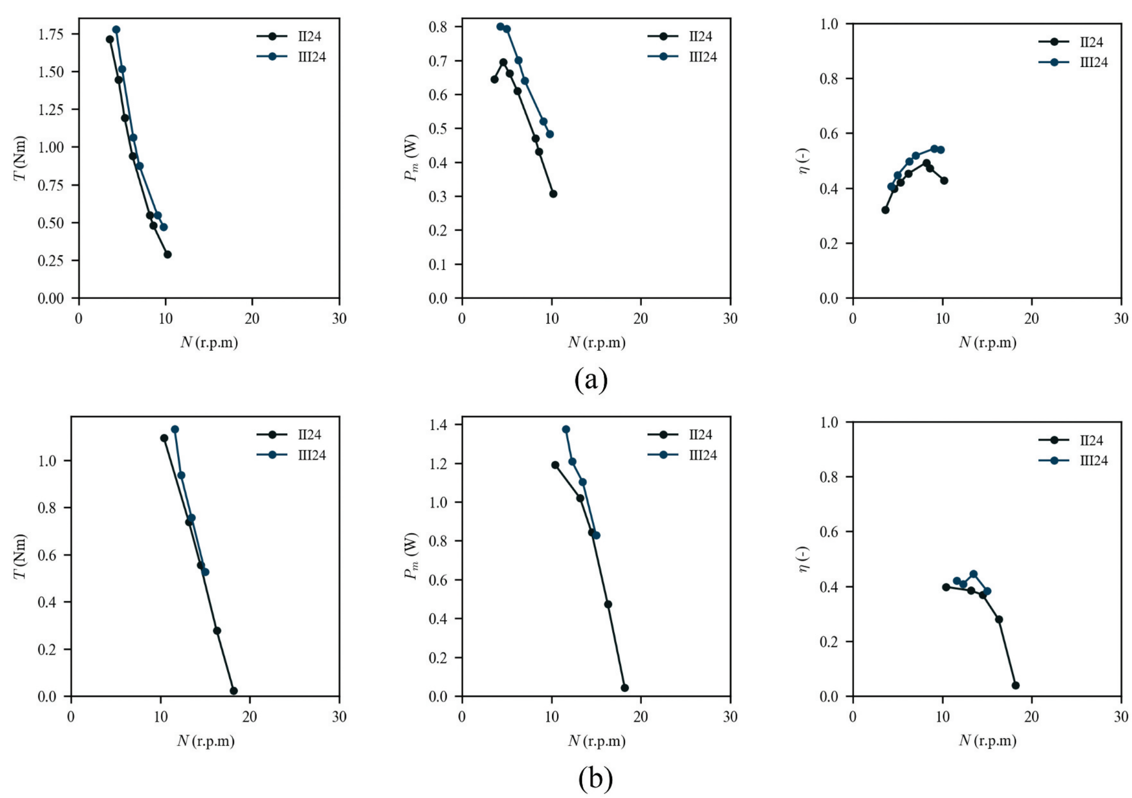

Figure 16. Experimental performance curves of the 24 curved blade wheel without (II24) and with a curved platform entry (III24) (torque, mechanical power and efficiency): (a) Q =1.83 L/s and (b) Q = 3.56 L/s.

observed for higher rotational speeds nor for higher flow rates, when there is increased turbulence or friction due to the increase in the number of blades. Additionally, minor differences are observed in the torque and the mechanical power curves for the 16 and 24-blade wheels as well as for 36 and 48-blade wheels, suggesting that these pairs of wheels have quite similar behaviours.

The maximum efficiency values (see Appendix A) are observed for the 36-blade wheel (61–63%), immediately followed by the 24-blade (54–62%), for both flow rates, suggesting that there is an optimal number of blades between 24 and 36 that leads to the maximum efficiency. The optimal rotational speed corresponding to the maximum efficiency varies significantly with the flow rate between 7 and 17 r.p.m. (see Appendix A). This suggests that the optimal rotational speed is strongly dependent on the flow rate as well as on the wheel and the flume bottom configurations.

Effect of the curvature of the blade

The purpose of the curved blades is to reduce head losses due to the impact of the blades on the tailrace and the impact of the entry water on the blades (Quaranta and Revelli 2015b). Therefore, it is expected that the use of curved blades, when well designed, produces better results in terms of mechanical power and efficiency. The performance curves obtained for two 24-blade wheels – the wheel with plane (I24) and the one with curved blades (II24) – are presented for two flow rate values in Figure 15.

Unlike expected, the wheel with curved blades (II24) has a lower efficiency than the wheel with plane blades (I24) for the same rotational speeds, despite the torque and the mechanical power being quite similar. This means that the curve-shape of the blades has not been well designed to mitigate the impact losses. A detailed analysis of the flow at the upstream side of the wheel shows increased turbulence at the wheel entry in comparison with the 24-plane blade wheel. This is due to the higher resistance and friction losses created by the impact angle of the curved blade on the water surface, as the blade edge is almost parallel to the water entry. Overall, the design of the curved blades should be improved based on the entry flow angle.

Effect of the curved entry platform

The purpose of the curved platform is to guide the flow and to limit the amount of leakage that occurs at the bottom of the flume. Therefore, it is expected that a curved platform located at the upstream entry will produce better results in terms of mechanical power and efficiency. This effect is more pronounced for wheels with fewer blades since these tend to have higher leakage at the bottom of the flume.

To analyze the effect of the curved platform, the results of two similar wheels are compared: the 24-blade wheel with curved blades without an upstream platform (II24) and with a curved upstream platform (III24). These results are presented in Figure 16.

As expected, the wheel III24 generates more torque and power than the wheel II24, at constant rotational speeds, and leads also to a higher efficiency. This means that the curved platform at the wheel entry significantly contributes to increase the harnessed mechanical power. This is because the entry curved platform reduces the volumetric water losses below the blades and, thus, increases the effective flow rate directed to the wheel. Overall, the curved bottom platform entry increases the wheel-harnessed power and mechanical efficiency.

Comparison of performance curves for a constant flow rate

The performance curves obtained for the six tested wheels and for $Q = 2.23$ L/s are presented Figure 17. The torque curves for wheels I16, I24, and II24 are very similar. However, increasing the number of blades for a constant rotational speed results in a higher torque: the wheel III24 produces higher torque than other wheels with 24 or fewer blades. This trend holds until a certain rotational speed is reached (15 r.p.m.), at which point the behaviour of the wheel significantly changes due to the added curved platform.

The mechanical power curves of the wheels I16, I24 and II24 are very similar. However, increasing the number of blades at a constant rotational speed appears to result in higher mechanical power. For the same rotational speed, the wheel III24 produces more mechanical power than the other wheels with 24 or fewer blades and it follows a similar trend to the other wheels. This trend holds until a certain rotational speed is reached (*ca.* 10 r.p.m. for a flow rate of 2.23 L/s), at which point the behaviour of the wheel significantly changes due to the added platform.

The efficiency trends of I16, I24, I36, I48, and II24 are similar, with the 36-bladed wheel achieving the highest efficiency. On

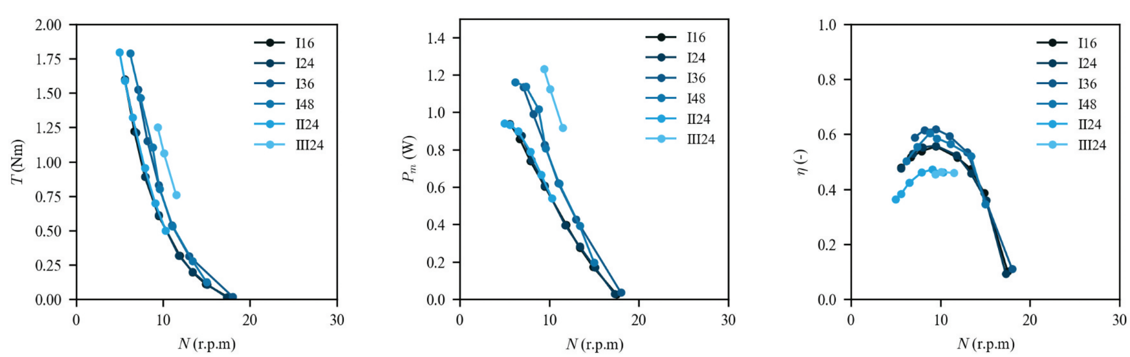

Figure 17. Experimental performance for the six wheels and Q = 2.23 L/s: torque, mechanical power and hydraulic efficiency.

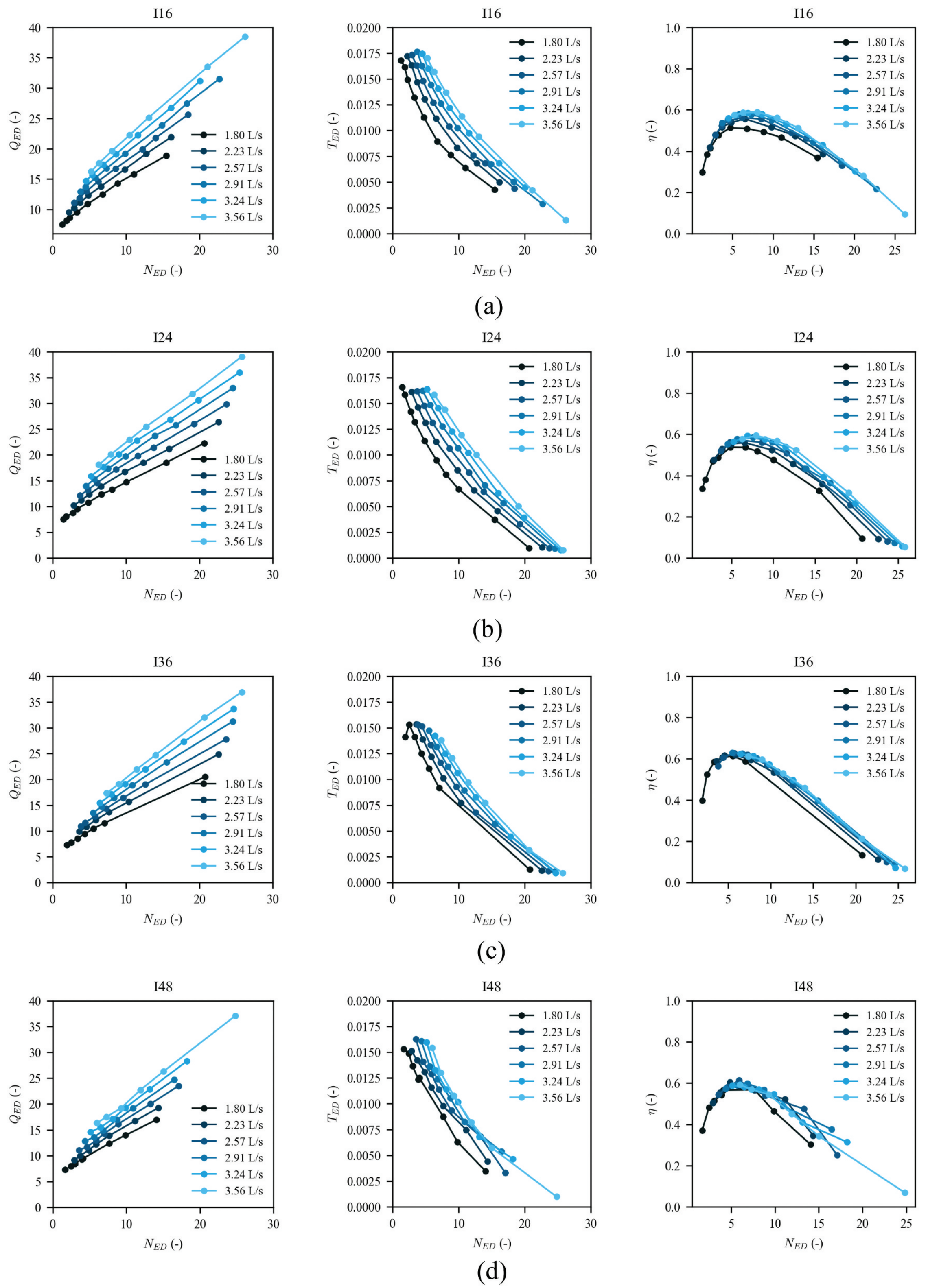

Figure 18. Non-dimensional performance curves of the four plane-blade wheels: $N_{ED} - Q_{ED}$, $N_{ED} - T_{ED}$and $N_{ED} - \eta$.

the other hand, the wheel III24 exhibits a constant efficiency between 10 and 15 r.p.m., after which it becomes the most efficient wheel. The optimal rotational speed (corresponding to the maximum efficiency) remains approximately constant, regardless of the number of blades or the blade curvature; the optimal rotational speed is around 10 r.p.m. for $Q = 2.23$ L/s.

Non-dimensional performance curves

The performance curves obtained for the four-plane wheel are also described in terms of the non-dimensional IEC factors (IEC 2019) respectively of rotational speed, discharge, torque and power, as follows:

$$N_{ED} = \frac{n \cdot D}{\sqrt{E}} \;;\; Q_{ED} = \frac{Q}{D^2 \cdot \sqrt{E}} \;;\; T_{ED} = \frac{T}{\rho D^3 E} \;;\; P_{ED} = \frac{P}{\rho D^2 \sqrt[3]{E}} \tag{5}$$

where n is the rotational speed (r.p.m), D is the wheel diameter (m) (in this case $D = 0.482$ m), E is the specific hydraulic energy described by $E = gH$ (J/kg), H is the wheel hydraulic head described by $H = H_u - H_d$, g is the gravity acceleration, and ρ the water density. These parameters allow to generalise results, though with parsimony, as the small size of the tested wheels has inevitable scale effects.

Accordingly, the performance curves $N_{ED} - Q_{ED}$, $N_{ED} - T_{ED}$ and $N_{ED} - \eta$ are presented in Figure 18. This figure shows that the shape of the non-dimensional factor curves is not significantly affected by the flow rate, having all the curves have similar trends despite showing a phase shift for flowrate. The efficiency curves tend to overlap except for the lowest discharge values. The maximum efficiency is achieved for the highest flow rate corresponding for each wheel to the following pair (N_{ED}, η) of values: I16 (6.3, 58%), I24 (7.9, 59.5%), I36 (5.5, 63%) and I48 (5.9, 61%).

Discussion

Concerning the effect of the number and shape of the blades and of the flume bottom, the obtained experimental results are consistent with previous research studies.

First, it is observed that increasing the number of blades until a certain value generally leads to higher torque and mechanical power and that there is a number of blades that leads to maximum efficiency; this is consistent with Müller and Kauppert (2004) and Quaranta and Revelli (2015b) observations, though efficiency differences are observed between the several studies mainly due to experimental conditions.

Secondly, Helzimar (2016) research highlighted the importance of the blade-shape in direct contact with the downstream water surface in affecting power output. The current results confirm this observation, as the experimental tests showed that the water depth upstream of the wheel is similar to the depth inside the wheel up to the blade in the vertical position. This indicates that the blade in direct contact with the downstream flow plays a crucial role in power generation. The fact is that the curved shape of the blades did not maximise the wheel efficiency, as the design of these blades did not take into consideration the direction of the flow entry to mitigate the impact losses and turbulence losses.

Thirdly, the obtained results confirmed that the curved flume bottom upstream of the water wheel has a key effect on the performance of the water wheel, strongly affecting the mechanical power and efficiency. These findings are aligned with the observations made by other researchers (Quaranta and Revelli 2015a, 2015b), which also noted improved wheel performance with similar inlet device configurations.

While these experimental tests contributed with valuable insights into the better understanding of the performance of undershot water wheels, notable differences in efficiency are observed when compared to findings from earlier studies conducted by researchers like Quaranta (2017), Müller and Kauppert (2004) and Helzimar (2016). In these studies, achieved efficiencies were approximately 90%, 87%, and 85%, respectively, for Quaranta (2017), Müller and Wolter (2004) and Helzimar (2016), while the present research observed a maximum efficiency of 63%. A plausible explanation is the influence of scale effects. The experimental tests were conducted at a different scale, where, for instance, the ratio between the lateral gap and the width of the flume was *c.a.* 10%. It is widely recognised that hydraulic performance can exhibit significant variations with changes in scale. Should these studies be pursued towards the development of a wheel prototype with a larger scale, it is expected to have lower friction losses in the wheel shaft, lower leakage and, consequently, higher hydraulic efficiencies.

Conclusions

The current research work aims at the theoretical and experimental investigation of the mechanical power and efficiency generated by undershot water wheels. An extensive experimental data collection programme was developed, and an extensive description of the setup and the instrumentation used to carry out the tests was presented. A total of 243 experimental tests were conducted to collect the physical data. Among these tests, approximately 48 tests were performed for each of the four wheels with 16, 24, 36, and 48 plane blades. Additionally, 26 tests were run for each of the three wheels with 24 curved blades, 24 curved blades and a curved inflow configuration, and 24 curved blades with a curved inflow configuration. The wheels were subjected to a range of rotational speeds, varying from 3 r.p.m. up until the rotational speed of the freewheel for each flow rate (15–21 r.p.m.). Some tests were discarded whenever the water depth exceeded the height of the blades or when the measured torque exceeded the maximum range value of the torque sensor. Consequently, it was not possible to obtain results for the complete range of rotational speeds as initially intended. A trend was observed in the hydraulic behaviour of the studied wheels that led to the characterization of upstream and downstream water depths.

An analysis is conducted on the experimental results of the six tested wheels, with a focus on the performance curves of torque, mechanical power and efficiency. This performance analysis concluded that, in general, the increase in the number of blades and the curved platform led to an increase in mechanical power and efficiency. On the other hand, the curved blades led to a decrease in performance. The maximum mechanical power output (1.8 W) was observed for the 48-plane blade wheel and a flow rate of 3.56 L/s. The corresponding rotational speed was *ca*. 11.5 r.p.m. with an associated hydraulic efficiency of 59.2%.

This research has provided several relevant contributions to the design of undershot water wheels: (i) the number of blades within the analysed range (16–48) that leads to the maximum efficiency is 36 (e.g. 63% for $Q = 2.83$ L/s), with an optimal rotational speed of 10 r.p.m. with a mechanical power of 1.45 W, being particularly relevant for lower flow rates (with efficiency differences up to 10%) and less important to higher flow rates (e.g. 59–61%, for $Q = 3.50$ L/s); (ii) the curvature of the blades strongly affects the efficiency of the wheel and should be designed to mitigate the friction losses created by the impact angle on the water surface, being demonstrated that not well-designed curved blades can decrease efficiency by 1/3 (e.g. 59% to 40%, for $Q = 3.50$ L/s); (iii) the flume bottom at upstream of the wheel should follow the wheel circumference to direct the flow towards the wheel and to minimize the water losses in the flume's bottom and walls; and (iv) the performance curves have been generalized using the international standard IEC 60,193: 2019 (IEC 2019) for impulse turbines to enable the utilization of the obtained results and performance curves in systems with different sizes and operating conditions.

Further investigation is necessary to understand the factors that contribute to the optimal rotational speed observed across a range of tested wheels with different blade numbers, blade curvature, and flume configurations. Full scale tests should be conducted to assess the impact of these factors in real-life conditions.

Acknowledgements

The authors would like to acknowledge Fundação para a Ciência e a Tecnologia (FCT) for funding the research project HORTO AQUAM SALUTAREM - WaterWise in Gardens in the Early Modern Period (grant number PTDC/HAR-HIS/28627/2017) and to Professor Ana Aurélio for the coordination and guidance of this project. The authors would like to thank Francisco Almeida for assembling the experimental facility and for his constant support and availability.

Disclosure statement

No potential conflict of interest was reported by the author(s).

Funding

This work was supported by the Fundação para a Ciência e a Tecnologia through the research Project PTDC/HAR-HIS/28627/2017, HORTO AQUAM SALUTAREM as well as through funding the research unit CERIS [UIDB/04625/2020].

ORCID

João Ferreira http://orcid.org/0000-0002-7889-9218
Dídia Covas http://orcid.org/0000-0001-6901-4767

References

Bekker, A., M. Van Dijk, and C. M. Niebuhr. 2022. "A Review of Low Head Hydropower at Wastewater Treatment Works and Development of an Evaluation Framework for South Africa." *Renewable and Sustainable Energy Reviews*: 159. https://doi.org/10.1016/j.rser.2022.112216.

Delgado, J., L. Andolfatto, D. I. C. Covas, and F. Avellan. 2019. "Hill Chart Modelling Using the Hermite Polynomial Chaos Expansion for the Performance Prediction of Pumps Running as Turbines." *Energy Conversion and Management* 187:578–592. https://doi.org/10.1016/j.enconman.2019.02.051.

Delgado, J., J. P. Ferreira, D. I. C. Covas, and F. Avellan. 2019. "Variable Speed Operation of Centrifugal Pumps Running as Turbines. Experimental Investigation." *Renewable Energy* 142:437–450. https://doi.org/10.1016/j.renene.2019.04.067.

Delgado, J. N. G. B. 2018. *Pumps Running as Turbines for Energy Recovery in Water Supply Systems*. École Polytechnique Fédérale de Lausanne. https://doi.org/10.5075/epfl-thesis-9036.

Elbatran, A. H., O. B. Yaakob, Yasser M. Ahmed, and H. M. Shabara. 2015. "Operation, Performance and Economic Analysis of Low Head Micro-Hydropower Turbines for Rural and Remote Areas: A Review." *Renewable and Sustainable Energy Reviews* 43:40–50. https://doi.org/10.1016/j.rser.2014.11.045.

Helzimar, H. 2016. "Turbine Wheel - a Hydropower Converter for Head Differences Between 2.5 and 5 M." PhD Thesis, University of Southampton. https://eprints.soton.ac.uk/400680/.

IEA. 2017. *World Energy Outlook*. France: International Energy Agency.

IEA. 2022. *World Energy Outlook*. International Energy Agency.

IEC. 2019. "IEC 60193: Hydraulic Turbines, Storage Pumps and Pump-Turbines - Model Acceptance Tests." International Electrotechnical Commission.

Jorge, Catarina, Maria Do Céu Almeida, and Dídia Covas. 2021. "Energy Balance in Wastewater Systems with Energy Recovery: A Portuguese Case Study." *Infrastructures* 6. 10. https://doi.org/10.3390/infrastructures6100141.

Jorge, Catarina, Maria Do Céu Almeida, Rita Salgado Brito, and Dídia Covas. 2022. "Water, Energy, and Emissions Nexus: Effect of Inflows in Urban Drainage Systems." *Water* 14 (6). https://doi.org/10.3390/w14060868.

Kelly-Richards, Sarah, Noah Silber-Coats, Arica Crootof, David Tecklin, and Carl Bauer. 2017. "Governing the Transition to Renewable Energy: A Review of Impacts and Policy Issues in the Small Hydropower Boom." *Energy Policy* 101:251–264. https://doi.org/10.1016/j.enpol.2016.11.035.

Kodirov, Dilshod, and Obid Tursunov. 2019. "Calculation of Water Wheel Design Parameters for Micro Hydroelectric Power Station." *E3S Web of Conferences*, 97. https://doi.org/10.1051/e3sconf/20199705042.

Laghari, J. A., H. Mokhlis, A. H. A. Bakar, and Hasmaini Mohammad. 2013. "A Comprehensive Overview of New Designs in the Hydraulic, Electrical Equipments and Controllers of Mini Hydro Power Plants Making it Cost Effective Technology." *Renewable and Sustainable Energy Reviews* 20:279–293. https://doi.org/10.1016/j.rser.2012.12.002.

Müller, Gerald, and Klemens Kauppert. 2004. "Performance Characteristics of Water Wheels." *Journal of Hydraulic Research* 42 (5): 451–460. https://doi.org/10.1080/00221686.2004.9641215.

Müller, Gerald, and Christian Wolter. 2004. "The Breastshot Waterwheel: Design and Model Tests." *Engineering Sustainability* 157 (ES4): 203–211. https://doi.org/10.1680/ensu.2004.157.4.203.

Oliveira, Pedro F. G., Nuno M. C. Martins, Pedro Fontes, and Dídia Covas. 2021. "Hydroenergy Harvesting Assessment: The Case Study of Alviela River." *Water* 13 (13). https://doi.org/10.3390/w13131764.

Quaranta, Emanuele. 2017. "Investigation and Optimization of the Performance of Gravity Water Wheels." PhD Thesis, Politecnico di Torino.

Quaranta, Emanuele, Amir Bahreini, Alireza Riasi, and Roberto Revelli. 2022. "The Very Low Head Turbine for Hydropower Generation in Existing Hydraulic Infrastructures: State of the Art and Future Challenges." *Sustainable Energy Technologies and Assessments*: 51. https://doi.org/10.1016/j.seta.2021.101924.

Quaranta, Emanuele, Riccardo Bergamin, and Anton J. Schleiss. 2023. "How to Estimate the Weight of Hydropower Electro-Mechanical Equipment? Available Evidence, Novel Equations and Challenges for Engineering

Applications." *Results in Engineering* 18. https://doi.org/10.1016/j.rineng.2023.101067.

Quaranta, Emanuele, and Gerald Müller. 2018. "Sagebien and Zuppinger Water Wheels for Very Low Head Hydropower Applications." *Journal of Hydraulic Research* 56 (4): 526–536. https://doi.org/10.1080/00221686.2017.1397556.

Quaranta, Emanuele, and Roberto Revelli. 2015a. "Output Power and Power Losses Estimation for an Overshot Water Wheel." *Renewable Energy* 83:979–987. https://doi.org/10.1016/j.renene.2015.05.018.

Quaranta, Emanuele, and Roberto Revelli. 2015b. "Performance Characteristics, Power Losses and Mechanical Power Estimation for a Breastshot Water Wheel." *Energy (Oxford)* 87:315–325. https://doi.org/10.1016/j.energy.2015.04.079.

Quaranta, Emanuele, and Roberto Revelli. 2017b. "Hydraulic Behavior and Performance of Breastshot Water Wheels for Different Numbers of Blades." *Journal of Hydraulic Engineering* 143. (1). https://doi.org/10.1061/(asce)hy.1943-7900.0001229.

Quaranta, Emanuele, and Roberto Revelli. 2018. "Gravity Water Wheels as a Micro Hydropower Energy Source: A Review Based on Historic Data, Design Methods, Efficiencies and Modern Optimizations." *Renewable and Sustainable Energy Reviews* 97:414–427. https://doi.org/10.1016/j.rser.2018.08.033.

Quaranta, E., and R. Revelli. 2016. "Optimization of Breastshot Water Wheels Performance Using Different Inflow Configurations." *Renewable Energy* 97:243–251. https://doi.org/10.1016/j.renene.2016.05.078.

Quaranta, E., and R. Revelli. 2017a. "CFD Simulations to Optimize the Blade Design of Water Wheels." *DrinkingWater Engineering Science* 10 (1): 27–32. https://doi.org/10.5194/dwes-10-27-2017.

Ramos, Helena M., Jorge G. Morillo, Juan A. Rodríguez Diaz, Armando Carravetta, and Aonghus McNabola. 2021. "Sustainable Water-Energy Nexus Towards Developing Countries' Water Sector Efficiency." *Energies* 14 (12). https://doi.org/10.3390/en14123525.

Ramos, Helena M., Charlotte Teyssier, Irene Samora, and Anton J. Schleiss. 2013. "Energy Recovery in SUDS Towards Smart Water Grids: A Case Study." *Energy Policy* 62:463–472. https://doi.org/10.1016/j.enpol.2013.08.014.

Sari, Dewi Puspita, Imam Syofii, Dendy Adanta, Anthony Costa, Muhammad Agil Fadhel Kurnianto, Sanjaya B. S. Nasution, Aji Putro Prakoso, and Fajar Sungging Rahmatullah. 2022. "Performance of Undershot Waterwheel in Pico Scale with Difference in the Blades Number." *Journal of the Brazilian Society of Mechanical Sciences and Engineering* 44 (3). https://doi.org/10.1007/s40430-022-03430-0.

Sinagra, Marco, Calogero Picone, Paolo Picone, Costanza Aricò, Tullio Tucciarelli, and Helena M. Ramos. 2022. "Low-Head Hydropower for Energy Recovery in Wastewater Systems." *Water* 14 (10). https://doi.org/10.3390/w14101649.

UN. 2015. *Transforming Our World: The 2030 Agenda for Sustainable Development: Resolution*. New York, USA: United Nations.

Williams, A. A., and R. Simpson. 2009. "Pico Hydro – Reducing Technical Risks for Rural Electrification." *Renewable Energy* 34 (8): 1986–1991. https://doi.org/10.1016/j.renene.2008.12.011.

APPENDIX A

Table A1. Summary of the experimental results for the wheel with 16 plane blades.

Pump frequency (Hz)	Q (L/s)	N (r.p.m.)	T (Nm)	h_u m)	h_d (m)	P_h (W)	P (W)	η (-)
25	1.79	2.7	1.95	0.155	0.020	1.86	0.55	0.30
25	1.82	3.7	1.65	0.142	0.021	1.67	0.64	0.38
25	1.81	4.3	1.36	0.130	0.021	1.48	0.61	0.41
25	1.81	5.6	0.98	0.114	0.022	1.21	0.58	0.48
25	1.83	7.1	0.66	0.098	0.023	0.96	0.49	0.51
25	1.83	8.9	0.40	0.084	0.025	0.73	0.37	0.51
25	1.83	10.1	0.26	0.073	0.028	0.56	0.27	0.49
25	1.83	11.4	0.18	0.066	0.029	0.45	0.21	0.47
25	1.83	13.4	0.08	0.058	0.032	0.32	0.12	0.37
25	1.83	15.4	0.01	0.052	0.034	0.21	0.02	0.12
30	2.22	4.6	1.93	0.157	0.024	2.22	0.93	0.42
30	2.23	5.6	1.60	0.143	0.025	1.95	0.94	0.48
30	2.23	6.7	1.22	0.129	0.026	1.66	0.86	0.52
30	2.24	7.9	0.89	0.114	0.026	1.37	0.74	0.54
30	2.24	9.5	0.61	0.099	0.028	1.08	0.60	0.56
30	2.26	11.9	0.32	0.083	0.031	0.77	0.40	0.52
30	2.26	13.4	0.20	0.073	0.033	0.58	0.28	0.47
30	2.26	14.9	0.11	0.066	0.035	0.45	0.17	0.39
30	2.27	17.5	0.01	0.057	0.036	0.27	0.03	0.10
34	2.56	6	1.91	0.160	0.027	2.51	1.20	0.48
34	2.55	7	1.54	0.144	0.028	2.16	1.13	0.52
34	2.57	8.1	1.20	0.131	0.029	1.85	1.02	0.55
34	2.57	9.7	0.81	0.114	0.030	1.47	0.83	0.56
34	2.56	11.7	0.51	0.098	0.032	1.11	0.62	0.56
34	2.57	14.1	0.26	0.083	0.035	0.79	0.39	0.49
34	2.57	14.8	0.20	0.077	0.036	0.66	0.31	0.46
34	2.58	16.6	0.09	0.069	0.038	0.48	0.16	0.33
34	2.59	18.5	0.02	0.062	0.039	0.33	0.04	0.11
38	2.89	7.5	1.83	0.159	0.029	2.68	1.44	0.54
38	2.89	8.4	1.50	0.146	0.031	2.38	1.32	0.55
38	2.90	9.9	1.08	0.129	0.032	1.94	1.12	0.58
38	2.89	11.3	0.78	0.115	0.033	1.59	0.92	0.58
38	2.90	13.3	0.49	0.100	0.036	1.23	0.68	0.55
38	2.90	16.2	0.21	0.083	0.038	0.80	0.35	0.44
38	2.90	17.3	0.12	0.075	0.040	0.60	0.21	0.35
38	2.90	18.7	0.05	0.069	0.040	0.46	0.10	0.22
38	2.91	19.7	0.02	0.066	0.041	0.38	0.04	0.10
42	3.25	8.9	1.76	0.160	0.033	2.92	1.64	0.56
42	3.23	9.9	1.40	0.146	0.034	2.53	1.45	0.58
42	3.21	11.4	1.00	0.129	0.035	2.03	1.19	0.59
42	3.22	13	0.72	0.116	0.037	1.68	0.97	0.58
42	3.22	15	0.42	0.100	0.039	1.25	0.67	0.53
42	3.23	17.4	0.21	0.087	0.041	0.88	0.38	0.43
42	3.23	18.6	0.10	0.078	0.042	0.65	0.20	0.30
42	3.23	20.7	0.02	0.072	0.043	0.49	0.05	0.11
46	3.54	10.2	1.67	0.160	0.035	3.10	1.78	0.58
46	3.54	11.3	1.31	0.146	0.036	2.65	1.56	0.59
46	3.54	13	0.92	0.129	0.038	2.13	1.25	0.59
46	3.54	14.9	0.60	0.113	0.040	1.66	0.93	0.56
46	3.55	16.5	0.39	0.102	0.041	1.31	0.67	0.51
46	3.53	19.9	0.10	0.082	0.044	0.73	0.20	0.28
46	3.53	21.5	0.02	0.076	0.045	0.55	0.05	0.09

Table A2. Summary of the experimental results for the wheel with 24 plane blades.

Pump frequency (Hz)	Q (L/s)	N (r.p.m.)	T (Nm)	h_u m)	h_d (m)	P_h (W)	P (W)	η (-)
25	1.79	3.1	1.94	0.154	0.021	1.88	0.63	0.34
25	1.81	3.7	1.66	0.142	0.022	1.70	0.64	0.38
25	1.81	5.1	1.25	0.127	0.022	1.43	0.67	0.47
25	1.81	5.7	0.99	0.115	0.022	1.21	0.59	0.49
25	1.81	7.3	0.67	0.098	0.023	0.95	0.51	0.54
25	1.83	8.8	0.43	0.085	0.024	0.74	0.40	0.54
25	1.83	10	0.32	0.078	0.026	0.65	0.34	0.52
25	1.84	11.2	0.22	0.071	0.028	0.53	0.25	0.48
25	1.85	13.8	0.08	0.060	0.031	0.34	0.11	0.33
25	1.86	15.4	0.01	0.053	0.033	0.24	0.02	0.09
30	2.18	4.9	1.92	0.156	0.024	2.20	0.98	0.45
30	2.23	5.6	1.60	0.144	0.025	1.97	0.94	0.48
30	2.24	6.9	1.21	0.129	0.025	1.66	0.88	0.53
30	2.23	8	0.89	0.114	0.026	1.35	0.75	0.55
30	2.25	9.5	0.61	0.100	0.027	1.09	0.61	0.56
30	2.25	11.8	0.32	0.082	0.030	0.75	0.39	0.52
30	2.25	13.4	0.20	0.075	0.032	0.62	0.28	0.46
30	2.25	15.1	0.11	0.068	0.034	0.47	0.17	0.36
30	2.26	17.3	0.02	0.059	0.036	0.31	0.03	0.09
34	2.55	6.1	1.91	0.159	0.027	2.49	1.22	0.49
34	2.56	7	1.50	0.143	0.027	2.11	1.10	0.52
34	2.56	8.3	1.15	0.129	0.028	1.78	1.00	0.56
34	2.56	9.5	0.84	0.115	0.029	1.46	0.84	0.57
34	2.58	11.6	0.50	0.097	0.031	1.08	0.60	0.56
34	2.58	13.5	0.29	0.084	0.033	0.81	0.41	0.51
34	2.58	14.8	0.19	0.079	0.036	0.70	0.30	0.43
34	2.59	17.1	0.07	0.069	0.037	0.47	0.12	0.26
34	2.59	18.4	0.02	0.063	0.038	0.36	0.03	0.08
38	2.89	7.5	1.83	0.159	0.029	2.68	1.44	0.54
38	2.89	8.4	1.45	0.145	0.030	2.31	1.28	0.55
38	2.89	9.6	1.10	0.130	0.031	1.92	1.11	0.58
38	2.89	11.3	0.74	0.113	0.032	1.50	0.87	0.58
38	2.92	13.1	0.49	0.100	0.034	1.18	0.67	0.56
38	2.92	15.3	0.22	0.084	0.037	0.82	0.35	0.43
38	2.92	17	0.14	0.079	0.039	0.69	0.25	0.36
38	2.93	19.5	0.02	0.068	0.040	0.43	0.03	0.07
42	3.24	8.8	1.73	0.159	0.032	2.85	1.59	0.56
42	3.23	9.5	1.40	0.146	0.032	2.47	1.39	0.56
42	3.22	11.2	1.00	0.128	0.033	1.98	1.17	0.59
42	3.23	12.9	0.66	0.112	0.035	1.55	0.89	0.58
42	3.25	14.6	0.43	0.100	0.037	1.22	0.66	0.54
42	3.25	17.3	0.19	0.087	0.040	0.88	0.35	0.39
42	3.24	18.8	0.09	0.079	0.041	0.67	0.18	0.27
42	3.24	20.5	0.01	0.072	0.042	0.49	0.03	0.06
46	3.54	10.1	1.65	0.159	0.034	3.03	1.74	0.58
46	3.54	11	1.26	0.144	0.035	2.52	1.45	0.58
46	3.55	12.5	0.93	0.128	0.036	2.04	1.21	0.59
46	3.56	14.5	0.60	0.112	0.038	1.59	0.90	0.57
46	3.56	15.9	0.41	0.102	0.040	1.29	0.68	0.52
46	3.57	19.1	0.13	0.086	0.043	0.83	0.26	0.32
46	3.58	21.1	0.01	0.076	0.044	0.56	0.03	0.05

Table A3. Summary of the experimental results for the wheel with 36 plane blades.

Pump frequency (Hz)	Q (L/s)	N (r.p.m.)	T (Nm)	h_u m)	h_d (m)	P_h (W)	P (W)	η (-)
25	1.75	3.7	1.69	0.157	0.020	1.87	0.74	0.40
25	1.75	5	1.62	0.144	0.020	1.65	0.87	0.52
25	1.75	5.8	1.23	0.128	0.020	1.36	0.80	0.59
25	1.77	6.8	0.91	0.113	0.020	1.14	0.69	0.61
25	1.77	7	0.66	0.101	0.021	0.95	0.58	0.61
25	1.78	10.1	0.45	0.089	0.022	0.78	0.46	0.59
25	1.79	11.6	0.02	0.054	0.032	0.25	0.03	0.13
30	2.16	13.7	1.68	0.157	0.023	2.18	1.09	0.50
30	2.17	15	1.52	0.144	0.024	1.93	1.13	0.59
30	2.17	6.2	1.15	0.129	0.024	1.61	0.99	0.62
30	2.20	7.4	0.83	0.114	0.025	1.34	0.83	0.62
30	2.19	8.8	0.54	0.099	0.026	1.05	0.62	0.59
30	2.20	9.6	0.31	0.085	0.028	0.80	0.43	0.53
30	2.22	11.1	0.02	0.060	0.035	0.33	0.04	0.11
34	2.48	13.4	1.65	0.156	0.027	2.39	1.35	0.56
34	2.49	15	1.45	0.145	0.027	2.13	1.29	0.61
34	2.50	17	1.04	0.128	0.028	1.74	1.09	0.63
34	2.51	7.3	0.74	0.114	0.029	1.43	0.89	0.62
34	2.52	9	0.45	0.098	0.030	1.10	0.63	0.57
34	2.53	10.4	0.25	0.086	0.032	0.83	0.39	0.47
34	2.51	11.2	0.02	0.064	0.037	0.38	0.04	0.10
38	2.83	12.7	1.61	0.157	0.030	2.63	1.57	0.60
38	2.83	15.3	1.34	0.144	0.030	2.30	1.45	0.63
38	2.84	16.8	1.01	0.130	0.031	1.95	1.22	0.62
38	2.84	18.1	0.70	0.116	0.032	1.59	0.96	0.60
38	2.85	8.8	0.42	0.101	0.033	1.20	0.65	0.54
38	2.88	10.7	0.18	0.085	0.035	0.81	0.32	0.40
38	2.88	11.9	0.02	0.069	0.039	0.45	0.04	0.09
42	3.19	13.3	1.56	0.158	0.033	2.87	1.75	0.61
42	3.16	14.8	1.24	0.144	0.033	2.46	1.53	0.62
42	3.19	17.4	0.90	0.130	0.034	2.05	1.26	0.61
42	3.19	19.6	0.62	0.116	0.035	1.65	0.95	0.57
42	3.20	10.2	0.36	0.101	0.036	1.26	0.62	0.50
42	3.20	12.1	0.13	0.085	0.038	0.81	0.25	0.31
42	3.19	13.7	0.02	0.074	0.041	0.53	0.04	0.07
46	3.49	14.8	1.40	0.155	0.036	2.96	1.75	0.59
46	3.49	16.7	1.16	0.145	0.036	2.61	1.60	0.61
46	3.49	18.7	0.84	0.131	0.037	2.17	1.29	0.60
46	3.50	20.5	0.51	0.114	0.038	1.64	0.87	0.53
46	3.50	11.6	0.32	0.102	0.039	1.30	0.59	0.46
46	3.51	13.2	0.08	0.085	0.040	0.79	0.17	0.21
46	3.51	15.3	0.02	0.077	0.043	0.59	0.04	0.07

Table A4. Summary of the experimental results for the wheel with 48 plane blades.

Pump frequency (Hz)	Q (L/s)	N (r.p.m.)	T (Nm)	h_u m)	h_d (m)	P_h (W)	P (W)	η (-)
25	1.79	3.7	1.92	0.159	0.024	2.01	0.74	0.37
25	1.81	5	1.58	0.142	0.024	1.72	0.83	0.48
25	1.81	5.8	1.29	0.130	0.024	1.53	0.78	0.51
25	1.81	6.8	0.97	0.116	0.024	1.27	0.69	0.54
25	1.81	7	0.96	0.115	0.023	1.24	0.70	0.57
25	1.83	10.1	0.40	0.084	0.026	0.74	0.42	0.57
25	1.84	11.6	0.23	0.075	0.027	0.59	0.27	0.47
25	1.85	13.7	0.09	0.063	0.029	0.41	0.12	0.30
25	1.86	15	0.01	0.057	0.032	0.31	0.02	0.07
30	2.18	6.2	1.79	0.158	0.028	2.31	1.16	0.50
30	2.23	7.4	1.47	0.145	0.028	2.05	1.14	0.55
30	2.24	8.8	1.10	0.127	0.028	1.69	1.02	0.60
30	2.23	9.6	0.80	0.113	0.029	1.38	0.81	0.59
30	2.25	11.1	0.53	0.099	0.029	1.10	0.62	0.57
30	2.25	13.4	0.28	0.082	0.032	0.75	0.39	0.52
30	2.25	15	0.13	0.073	0.032	0.57	0.20	0.35
30	2.26	17	0.01	0.063	0.034	0.38	0.02	0.06
34	2.55	7.3	1.80	0.158	0.029	2.52	1.37	0.55
34	2.56	9	1.39	0.146	0.031	2.26	1.31	0.58
34	2.56	10.4	1.04	0.128	0.031	1.85	1.14	0.61
34	2.56	11.2	0.76	0.115	0.032	1.52	0.89	0.58
34	2.58	12.7	0.49	0.102	0.032	1.22	0.66	0.54
34	2.58	15.3	0.24	0.083	0.035	0.79	0.38	0.47
34	2.59	16.8	0.08	0.074	0.035	0.58	0.15	0.25
34	2.59	18.1	0.01	0.067	0.036	0.45	0.03	0.06
38	2.89	8.8	1.70	0.158	0.031	2.73	1.57	0.57
38	2.89	10.7	1.28	0.145	0.034	2.43	1.44	0.59
38	2.89	11.9	0.97	0.131	0.034	2.03	1.21	0.60
38	2.89	13.3	0.64	0.113	0.036	1.56	0.89	0.57
38	2.92	14.8	0.39	0.101	0.036	1.25	0.61	0.49
38	2.92	17.4	0.16	0.082	0.038	0.75	0.28	0.38
38	2.93	19.6	0.02	0.070	0.040	0.48	0.04	0.08
42	3.24	10.2	1.63	0.159	0.034	2.96	1.74	0.59
42	3.23	12.1	1.20	0.146	0.037	2.62	1.52	0.58
42	3.22	13.7	0.84	0.130	0.037	2.11	1.20	0.57
42	3.23	14.8	0.59	0.115	0.039	1.68	0.92	0.55
42	3.25	16.7	0.29	0.099	0.039	1.22	0.50	0.41
42	3.25	18.7	0.13	0.084	0.041	0.79	0.25	0.31
42	3.24	20.5	0.02	0.075	0.042	0.55	0.04	0.07
46	3.54	11.6	1.51	0.159	0.037	3.09	1.83	0.59
46	3.54	13.2	1.10	0.145	0.038	2.68	1.53	0.57
46	3.55	15.3	0.76	0.131	0.040	2.24	1.22	0.55
46	3.56	16.7	0.42	0.112	0.040	1.62	0.73	0.45
46	3.56	18.2	0.22	0.099	0.041	1.21	0.42	0.34
46	3.58	21.4	0.02	0.079	0.043	0.62	0.04	0.07

Table A5. Summary of the experimental results for the wheel with 24 curved blades.

Pump frequency (Hz)	Q (L/s)	N (r.p.m.)	T (Nm)	h_u m)	h_d (m)	P_h (W)	P (W)	η (-)
25	1.80	3.6	1.71	0.158	0.025	2.02	0.65	0.32
25	1.80	4.6	1.44	0.143	0.024	1.75	0.70	0.40
25	1.81	5.3	1.19	0.133	0.024	1.57	0.66	0.42
25	1.81	6.2	0.94	0.121	0.023	1.35	0.61	0.45
25	1.82	8.2	0.55	0.099	0.022	0.95	0.47	0.49
25	1.84	8.6	0.48	0.096	0.023	0.91	0.43	0.47
25	1.83	10.2	0.29	0.083	0.025	0.72	0.31	0.43
25	1.86	13.9	0.03	0.060	0.029	0.35	0.04	0.11
30	2.21	5	1.80	0.169	0.029	2.58	0.94	0.36
30	2.22	5.6	1.59	0.162	0.029	2.43	0.93	0.38
30	2.23	6.5	1.32	0.148	0.028	2.12	0.90	0.42
30	2.24	7.9	0.95	0.130	0.026	1.71	0.79	0.46
30	2.24	9.1	0.70	0.116	0.026	1.41	0.67	0.47
30	2.24	10.3	0.50	0.105	0.027	1.17	0.54	0.46
30	2.25	12.2	0.28	0.090	0.028	0.89	0.36	0.40
30	2.26	13.5	0.17	0.082	0.029	0.74	0.24	0.32
30	2.29	15.3	0.03	0.068	0.032	0.48	0.04	0.08
38	2.86	8.6	1.30	0.163	0.033	2.91	1.17	0.40
38	2.90	10.1	0.95	0.144	0.032	2.37	1.01	0.42
38	2.89	10.9	0.81	0.135	0.032	2.12	0.92	0.44
38	2.90	12.7	0.52	0.118	0.033	1.66	0.69	0.41
38	2.89	14.3	0.31	0.105	0.034	1.32	0.47	0.35
38	2.93	16.5	0.02	0.083	0.036	0.78	0.04	0.05
46	3.20	10.4	1.09	0.160	0.035	3.00	1.19	0.40
46	3.50	13.2	0.74	0.145	0.038	2.65	1.02	0.38
46	3.52	14.5	0.56	0.133	0.038	2.28	0.84	0.37
46	3.53	16.3	0.28	0.115	0.039	1.70	0.47	0.28
46	3.56	18.2	0.02	0.096	0.040	1.10	0.04	0.04

Table A6. Summary of the experimental results for the wheel with 24 curved blades with a curved platform.

Pump frequency (Hz)	Q (L/s)	N (r.p.m.)	T (Nm)	h_u m)	h_d (m)	P_h (W)	P (W)	η (-)
25	1.79	4.3	1.78	0.157	0.023	1.97	0.80	0.41
25	1.79	5	1.52	0.146	0.022	1.77	0.79	0.45
25	1.84	6.3	1.06	0.126	0.021	1.41	0.70	0.50
25	1.82	7	0.87	0.117	0.021	1.24	0.64	0.52
25	1.84	9.1	0.55	0.098	0.024	0.96	0.52	0.54
25	1.84	9.8	0.47	0.093	0.025	0.89	0.48	0.54
25	1.86	11.2	0.37	0.087	0.027	0.80	0.44	0.55
30	2.21	5.9	1.77	0.165	0.027	2.47	1.09	0.44
30	2.24	8.2	0.98	0.131	0.025	1.69	0.84	0.50
30	2.25	9.6	0.71	0.116	0.026	1.40	0.72	0.51
30	2.25	14.2	0.32	0.091	0.031	0.94	0.48	0.51
30	2.28	16.6	0.26	0.087	0.033	0.87	0.45	0.52
38	2.88	9.4	1.25	0.158	0.031	2.71	1.23	0.45
38	2.88	10.1	1.06	0.148	0.031	2.43	1.12	0.46
38	2.89	11.5	0.76	0.132	0.031	1.99	0.92	0.46
38	2.92	13.5	0.51	0.116	0.033	1.61	0.72	0.45
46	3.52	11.6	1.13	0.164	0.036	3.26	1.38	0.42
46	3.50	12.3	0.94	0.155	0.037	2.96	1.21	0.41
46	3.54	15	0.53	0.130	0.038	2.16	0.83	0.38